



كلية الهندسة
College of Engineering
QATAR UNIVERSITY جامعة قطر

BACHELOR OF SCIENCE DEGREE IN ELECTRICAL ENGINEERING

Senior Design Project Report

Department of Electrical Engineering
Qatar University

Qatar University First Solar Car to Compete in the World Solar Challenge: Design of Energy Management System

Report by

Mariam Sherif EIMenshawy

Mena Sherif EIMenshawy

Supervisor

Dr. Ahmed Massoud

Co-Supervisor

Prof. Adel Gastli

Date

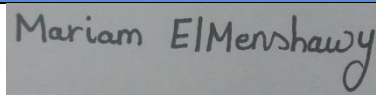
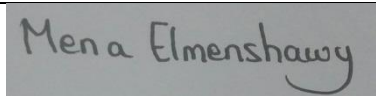
24/05/2016

DECLARATION STATEMENT

We, the undersigned students, confirm that the work submitted in this project report is entirely our own and has not been copied from any other source. Any material that has been used from other sources has been properly cited and acknowledged in the report.

We are fully aware that any copying or improper citation of references/sources used in this report will be considered plagiarism, which is a clear violation of the Code of Ethics of Qatar University.

In addition, we have read and understood the legal consequences of committing any violation of the Qatar University's Code of Ethics.

	Student Name	Student ID	Signature	Date
1	Mariam ElMenshawy	201105930		24/5/2016
2	Mena Elmenshawy	201203675		24/5/2016

ABSTRACT

The first solar car racing named as the World Solar Challenge was organized in Australia aiming to trigger the development of solar powered vehicles by researchers all over the world, and so do, various technologies have emerged targeting to make solar powered vehicles perform similar to fuel powered vehicles. Nevertheless, such vehicles still have limitations in terms of energy management technology, including photovoltaic and energy storage system technology. The term energy management means the effective and wise use of energy that result in maximizing the system efficiency. Generally, a solar car energy management system must ensure that the flow of electrical power from the PV and from/to the energy storage devices to the motor are optimized and monitored. In this report, few landmarks in development and evolution of solar car races by teams from different universities and international institutes are introduced showing the noticeable improvements in the car's energy efficiency.

Nowadays, solar cars are built by student groups that cooperate from different disciplines for the purpose of racing; encouraging alternative energy usage awareness. The car should be designed for reliability since it must operate successfully for several days (seven day race) and under harsh environmental conditions such as: temperature, humidity, and pressure. Energy efficiency and light weight are important factors for a successful vehicle. To achieve that, a 5 kWh Lithium ion battery, 2 kW in-wheel axial flux permanent magnet brushless DC motor with a rated voltage of 48 V, and 1035 W monocrystalline PV modules are selected to attain such conditions. In addition, ultra-capacitors are used as a second energy storage device to take the advantages of the fast charging and discharging and maximize the efficiency by storing the energy generated during frequent starts and stops of the solar car rather than wasting it. Since the main goal is to transfer power from the three sources which are PV panel, battery, and ultra-capacitors to the motor in an efficient way, Buck-Boost converters are designed and implemented to regulate the output voltage of the three sources so that it matches the voltage of the DC bus. The designed and implemented system is an open-loop control system.

To draw the maximum power from the PV modules, PV module I-V and P-V characteristics are studied under the effect of solar insolation and temperature by simulating the PV model using Matlab/Simulink. In addition, the maximum power point tracker model is modeled and implemented using perturb and observe technique to select the optimum point. Moreover, different energy management cases are considered under different operating conditions using the three sources mentioned earlier that supply the load according to its power requirements. Furthermore, the overall system is analyzed by doing performance assessment to observe the effect of varying the load on the voltage, current, and power at each node in the system, as well as the efficiency of each converter. Consequently, the designed converters are found to operate at low efficiency that does not exceed 70%, and this is because they are designed to operate at high power ratings, however they are not. Reasons for obtaining such results are investigated and illustrated in chapter 5.

ACKNOWLEDGEMENTS

Firstly, we would like to express our sincere gratitude to the supervisors, **Dr. Ahmed Massoud** and **Prof. Adel Gastli**, for their continuous support of our senior design project, for their patience, motivation, and immense knowledge. Their devoted time guidance, and insightful comments helped us in all the time of research, project development, and writing of this report.

Our sincere thanks also go to **Eng. Hamid Azani** for his generous help. Also, we would like to thank **Mr. Ayman Ammar** and **Mr. Mohammed Ayad** for their great effort.

Finally, special thanks to our **parents** for supporting us spiritually throughout this project and our life in general.

TABLE OF CONTENTS

Chapter 1 : Introduction	1
1.1 Background & Problem Definition	1
1.2 Objectives	3
1.3 Project Plan.....	4
Chapter 2 : Literature Review	6
2.1 History of solar cars.....	6
2.2 Evolution of solar car races	7
2.3 World solar challenge.....	9
2.4 Main components of solar car.....	10
2.4.1 Solar Arrays:.....	10
2.4.2 Maximum Power Point Tracker:	11
2.4.3 Energy Storage System:.....	11
2.4.4 Electric Motor:	14
2.5 Constraints.....	15
Chapter 3 : PV & Maximum Power Point Tracking.....	17
3.1 PV Modeling.....	17
3.1.1 PV Hierarchy:	17
3.1.2 PV Cell Model:.....	18
3.1.3 PV Module & PV Array Model:	19
3.1.4 Mathematical Models of PV Module & PV Array:.....	21
3.1.5 Results and Discussion:.....	23
3.2 MPPT Modelling using Perturb and Observe Technique	26
3.2.1 P&O Algorithm:.....	26
3.2.2 P&O Flowchart:	27
3.2.3 Model of MPPT:.....	28
Chapter 4 : Design of Solar Car Electrical System.....	29
4.1 Solar Panel	29

4.2	Battery Pack.....	30
4.3	DC/DC Converters	30
4.3.1	Buck-Boost Converter for PV Panel (MPPT):	32
4.3.2	Buck-Boost Converter for Battery.....	33
4.5.1	Buck-Boost Converter for Ultra-capacitors:	34
4.4	Electric Motor	34
4.5	Steady state analysis of energy management system (EMS).....	36
4.6	Topologies	39
Chapter 5 : Practical Implementation		40
5.1	Controller	40
5.2	Gate Drive Circuit.....	40
5.3	Voltage & Current Transducers	41
5.4	Software.....	41
5.5	Hardware	43
5.6	Results & Discussion.....	44
5.6.1	Buck-Boost Converter:.....	44
5.6.2	Maximum Power Point Tracker MPPT:.....	45
5.6.3	Energy Management System:.....	47
5.6.4	Performance Assessment:.....	55
5.7	Project's Cost.....	56
5.8	Design Limitations	56
Chapter 6 : Conclusion and Future Work		58

LIST OF FIGURES

Figure 1-1 System architecture.	3
Figure 1-2 Gantt chart summarizing all the tasks done in SDP I.	4
Figure 1-3 Gantt chart summarizing all the tasks done in SDP II.	5
Figure 2-1 Few landmarks in the development of solar cars.	6
Figure 2-2 Development of solar cars: (a) Sunmobile by William G. Cobb; (b) The first full-sized solar car by the International Rectifier Company; (c) Bluebird by Edward Passerini [5].....	7
Figure 2-3 Sunraycer vehicle by General Motors [9].....	7
Figure 2-4 Average speeds of the cars participated in the challenger class for previous WSC events.	9
Figure 2-5 The Winning cars in the challenger class for previous WSC events from 1987 to 2013.	10
Figure 2-6 Battery Management System.	13
Figure 3-1 Equivalent circuit of a PV cell.	18
Figure 3-2 Generalized array model.....	20
Figure 3-3 Approximate array model.	20
Figure 3-4 Simplified array model.	21
Figure 3-5 Mathematically modelled PV module interfaced to the physical ports.....	22
Figure 3-6 Simulink model of a PV module illustrating the I-V and P-V output characteristics.	22
Figure 3-7 Mathematically modelled PV array interfaced to the physical ports.	22
Figure 3-8 I-V output characteristics with different values of solar insolation at constant temperature level of 25°C.....	24
Figure 3-9 P-V output characteristics with different values of solar insolation at constant temperature level of 25°C.....	24
Figure 3-10 I-V output characteristics with different values of operating temperature at constant insolation level of 1kW/m ²	25
Figure 3-11 P-V output characteristics with different values of operating temperature at constant insolation level of 1kW/m ²	25

Qatar University First Solar Car to Compete in the World Solar Challenge: Design of Energy Management System

Figure 3-12 PV conversion system.....	26
Figure 3-13 P&O algorithm.	27
Figure 3-14 P&O flowchart [27].....	27
Figure 3-15 PV module voltage, current, and power curves at insolation level of 1 kW/m ² and temperature level of 25°C.....	28
Figure 4-1 Switched mode DC/DC converters.....	30
Figure 4-2 Buck Converter.....	31
Figure 4-3 Boost Converter.....	31
Figure 4-4 Buck-Boost Converter.....	31
Figure 4-5 Ripple output voltage, inductor voltage and current waveforms for Buck-Boost converter.....	33
Figure 4-6 Radial flux permanent magnet machine [36].....	35
Figure 4-7 Axial flux permanent magnet machine [36].....	35
Figure 4-8 Single motor driving the wheels through a gearbox drive shaft.	35
Figure 4-9 Two in-wheel hub motors driving the wheels through very small drive shafts.	36
Figure 4-10 Energy management.....	37
Figure 4-11 EMS flowchart.	38
Figure 4-12 First topology.....	39
Figure 4-13 Second topology.....	39
Figure 5-1 Gate drive board.....	41
Figure 5-2 Matlab/Simulink simulation for generating the PWM signal for tracking the PV MPP.	42
Figure 5-3 Test rig.....	43
Figure 5-4 Overall system hardware connections.....	43
Figure 5-5 Output voltage and its ripple, Inductor current and voltage waveforms.....	44
Figure 5-6 PV array power, voltage, and current waveforms at the MPP with 10 W/div, 10 V/div, and 1 A/div respectively, and with a perturb size of 10 ⁻⁷	45

Figure 5-7 MPPT results at perturb size of 10^{-7} : (a) P-V curve at variable duty cycle; (b) Maximum power point.....	45
Figure 5-8 PV array power, voltage, and current waveforms at the MPP with 4 W/div, 20 V/div, and 200 mA/div respectively, and with a perturbation size of 0.01.....	46
Figure 5-9 PV array power, voltage, and current waveforms at the MPP with 4 W/div, 20 V/div, and 200 mA/div respectively, and with a perturbation size of 10^{-7}	46
Figure 5-10 Charging case single line diagram.....	48
Figure 5-11 IGBT Module losses.....	49
Figure 5-12 Discharging case single line diagram.	51
Figure 5-13 Discharging case single line diagram where the PV power is zero and the battery is discharged to feed the load.....	52
Figure 5-14 Discharging case single line diagram where the battery is charging the ultra-capacitors.	54
Figure 5-15 Ultra-capacitor's voltage before and after charging.....	54
Figure 5-16 Single line diagram showing performance assessment for the energy management.	55
Figure 6-1 Multiport system structure.	60

LIST OF TABLES

Table 2-1 Four generations for a sample of a solar car that participated in the ASC [7].....	8
Table 2-2 World Solar Challenge classes [11].....	9
Table 2-3 Basic components of solar car [3].....	10
Table 2-4 Comparison between the widely used solar cells [15].	11
Table 2-5 2015 World Solar Challenge approved battery chemistry and mass [3].....	12
Table 2-6 Comparison between batteries and ultra-capacitors.	14
Table 2-7 Battery weight limitations.....	16
Table 3-1 Solarex MSX 60 PV module specifications at 1 kW/m ² and 25 °C [14].	23
Table 4-1 X series solar panel specifications.....	29
Table 4-2 Third design of the Buck-Boost converter for PV.	32
Table 4-3 Prototype design of the Buck-Boost converter for PV.	32
Table 4-4 Design of the Buck-Boost converter for Battery.	33
Table 4-5 Prototype design of the Buck-Boost converter for Battery.	33
Table 4-6 Design of the Buck-Boost converter for Ultra-capacitors.	34
Table 4-7 Prototype design of the Buck-Boost converter for Ultra-capacitors.....	34
Table 4-8 Different conditions of the power flow according to the load conditions.	38
Table 5-1 System parameters.....	44
Table 5-2 Project's cost.	56

GLOSSARY

List of Abbreviations			
ICE	Internal Combustion Engine	BMS	Battery Management System
HEVs	Hybrid Electric Vehicles	SoC	State of Charge
BEVs	Battery Electric Vehicles	SoH	State of Health
PV	Photovoltaic	SoL	State of Life
EVs	Electric Vehicles	BLDC	Brushless Direct Current
QU	Qatar University	PWM	Pulse Width Modulation
DC	Direct Current	AC	Alternating Current
MPPT	Maximum Power Point Tracker	P&O	Perturb and Observe
MPP	Maximum Power Point	RFPM	Radial Flux Permanent Magnet
WSC	World Solar Challenge	AFPM	Axial Flux Permanent Magnet
GM	General Motors	PMs	Permanent Magnets
DoE	Department of Energy	IWM	In-Wheel Motor
ASC	American Solar Challenge	EMS	Energy Management System
CdTe	Cadmium Telluride	DSC	Digital Signal Controller
CIS/CIGS	Cadmium Indium Gallium Selenide	DSP	Digital Signal Processor
BPS	Battery Protection System	A/D	Analog to Digital
Li	Lithium	I/O	Input/Output
Li-Po	Lithium Polymer	GND	Ground
Pb	Lead	IGBT	Insulated-Gate Bipolar Transistor
Ni-MH	Nickel Metal Hydride	MCU	Micro Controller Unit
LiFePO4	Lithium Iron Phosphate	MPEI	Multiport Power Electronic Interface

List of Symbols			
I_{PH}	Light-generated current or photocurrent	f_s	Switching Frequency
I_S	Cell saturation of dark current	T_s	Switching Time
Q	Electron charge ($=1.6 \times 10^{-19}$ C)	Δi_L	Ripple Inductor Current
K	Boltzmann constant ($= 1.38 \times 10^{-23}$ J/K)	V_r/V_o	Ripple Output Voltage
T	Cell working temperature	D	Duty Cycle
A	Ideal factor (dependent on PV technology)	I_L	Average Inductor Current
R_{SH}	Shunt resistance	L_{design}	Designed Inductor Value
R_S	Series resistance	v_L	Rated Inductor Voltage
I_{SC}	Cell short-circuit current at a 25 °C and 1 kW/m ²	$\Delta i_{L,new}$	Updated Ripple Inductor Current
K_I	Cell short-circuit current temperature coefficient	$I_{L,rms}$	RMS Inductor Current
T_r	Cell reference temperature	C_{design}	Designed Capacitor Value
λ	Solar insolation in kW/m ²	V_r/V_o_{new}	Updated Ripple Output Voltage
I_{RS}	Cell reverse saturation current at a reference temperature and a solar radiation	V_C	Rated Capacitor Voltage
E_G	Band-gap energy of the semiconductor used in the cell	V_d	Rated Diode Voltage
V_{OC}	PV open-circuit voltage at the reference temperature	V_s	Rated Switch Voltage
N_S N_P	Series number for a PV array Parallel number for a PV array	K_{Load}	Sign of the load current
K_{PV}	Sign of the PV current	I_{PV}	PV array contribution in the DC bus
K_B	Sign of the battery current	I_B	Battery contribution in the DC bus
K_C	Sign of the ultra-capacitor current	I_C	Ultra-capacitor contribution in the DC bus
I_{Load}	Load Current		

Chapter 1 : INTRODUCTION

This chapter describes the background & problem definition illustrating the gradual shift from producing conventional vehicles to solar powered electric vehicles due to the urgent need to decarbonise the world economy. Also, the objectives are specifically stated clarifying the main goal of this project.

1.1 Background & Problem Definition

The automotive industry has been dominated by the internal combustion engines (ICEs) powered vehicles, which are the technological solution that has created the global organization of transport systems [1]. This industry is witnessing a gradual shift from manufacturing conventional vehicles powered by ICE to less carbon-intensive drive technologies, including hybrid and battery electric vehicles (HEVs and BEVs) that are gaining competitive advantages and attracting considerable investments. Consequently, innovative transportation services will invade in the long run, where traditional cars will lose their previous importance, since the new alternatives no longer require the core technologies of conventional vehicles such as ICEs and gearboxes [1]. HEVs contain ICE supported by an electric motor, and a battery of limited capacity that acts as a temporary complementary source assisting the engine or replacing it at low speed [1]. The battery charging process takes place via the electricity generated by the engine and the recuperation of brake energy. However, BEVs contain an electric motor with batteries for storage purposes. Batteries are charged from grid electricity, brake energy recuperation, and from renewable energy sources as photovoltaic panels [1].

Accordingly, research and development in the area of renewable energy are expanding significantly, owing to increasing sustainability and environmental awareness. Among the renewable energy resources, solar energy through PV panels has been the most attractive, due to its low installation costs, ease of maintenance and the fact that the generation of electricity in that way is rather clean. Solar energy is a convenient energy supply with great long-term benefits relative to oil prices; in addition, it is extensively available and totally free of charge, despite the sunlight intermittency. To further improve energy efficiency, several electric power applications have recently used PV array systems, where the idea of installing PVs on EVs has emerged resulting in solar powered electric vehicles.

Solar cars are the upcoming vehicles of the automobile industry in the long run; they are eco-friendly since they provide less pollution [2]. Besides, solar vehicles require less maintenance when compared to the conventional vehicles. Solar cars, like many student engineering projects, showcase innovation, technology development, applicable solutions, and carry on an engineering legacy [3]. The building of solar vehicles is now referred to as "brain sport" [3]. Designing, developing and testing solar powered vehicles will introduce new methods to improve and integrate systems from experimental solar cars to marketable cars.

Fortunately, nowadays solar cars are built by student groups that cooperate from different disciplines to develop the most efficient solar cars possible for the purpose of racing which is growing at a tremendous rate around the world. Solar vehicle competition is an environment in which technology has been built for research. The World Solar Challenge held in Australia is one of the events that have been organizing the world solar car competition every two years where teams from leading international universities and technical institutes, together with private entrepreneurs, come together to test and promote the ultimate synergy of nature, motion and innovation. The race aims to promote solar energy usage, to encourage energy sufficient technology development, such as PV cells, batteries, electric motors and lightweight vehicles, and to show the need of good energy management strategies.

1.2 Objectives

Solar cars development process still has restrictions specifically in terms of energy management technology [4]. The objective of this project is to maximize the system efficiency through the effective usage of energy that includes PV and energy storage systems technologies. These two technologies should be designed in order to ensure that the flow of electrical power from the PV and storage devices to the loads will be observed and optimized [4].

Qatar University students' long term objective is to design the first QU solar car which will be able to compete in future World Solar Challenges. The team should be made up of electrical and mechanical engineering students from both departments in order to design and control the energy management system and to do the mechanical design respectively. However, the short term objective is to design the energy management system of the solar car resulting in high energy efficiency to be a starter point for regular participation in future races.

As shown in Figure 1-1, DC/DC converters are the main building blocks in this project. Since the PV cells are energy converters and not energy storage devices, or in other words, PV cells supply energy, thus a unidirectional converter for maximum power point tracking (MPPT) should be designed for maximum power point operation of the PV. On the other hand, batteries and ultra-capacitors are energy storage devices that are charged and discharged according to the energy management system, thus bidirectional converters should be designed to manage the energy and regulate the voltage of both batteries and ultra-capacitors so that they match the load voltage requirements.

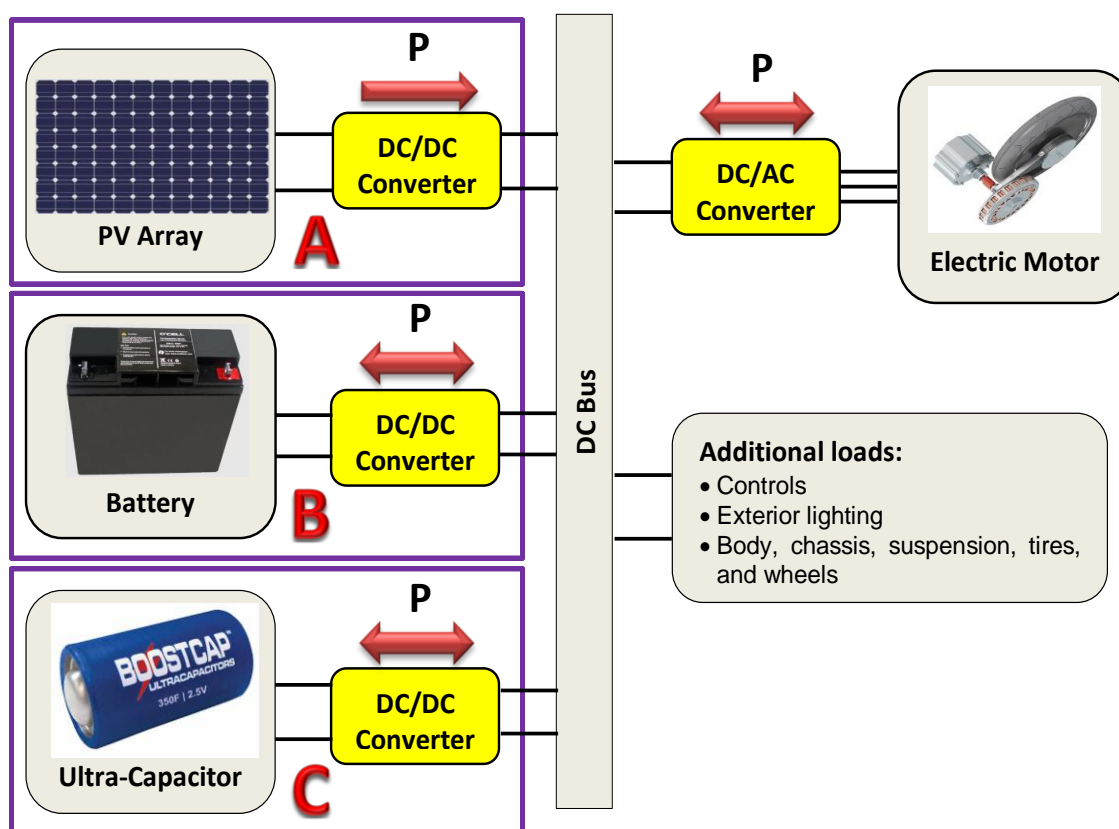


Figure 1-1 System architecture.

1.3 Project Plan

In this section the whole project tasks including SDP I and SDP II are listed. Gantt charts are used to illustrate the time slot assigned for each task.

The main tasks for SDP I are summarized as follows:

- 1) PV modeling using Matlab/Simulink.
- 2) Searching for the main components of solar cars.
- 3) Setting the design constraints according to the World Solar Challenge regulations.
- 4) Looking for the history of solar cars and the evolution of solar car races.
- 5) Designing the electrical system of the solar car by reviewing the PV panels', batteries', and motors' technologies available in the market.
- 6) Designing the DC/DC converters (Unidirectional Buck-Boost converter for the PV, Bidirectional Buck-Boost converter for the battery, and Bidirectional Buck-Boost converter for the ultra-capacitors).
- 7) Simulating the DC/DC converters using Matlab/Simulink.
- 8) Maximum Power Point Tracker modeling using Perturb & Observe algorithm by Matlab/Simulink.
- 9) PCB designs of the DC/DC converters using DipTrace.
- 10) Implementing the unidirectional Buck-Boost converter for the PV.
- 11) Implementing the bidirectional Buck-Boost converter for the battery.
- 12) Studying the steady-state analysis of Energy Management System.

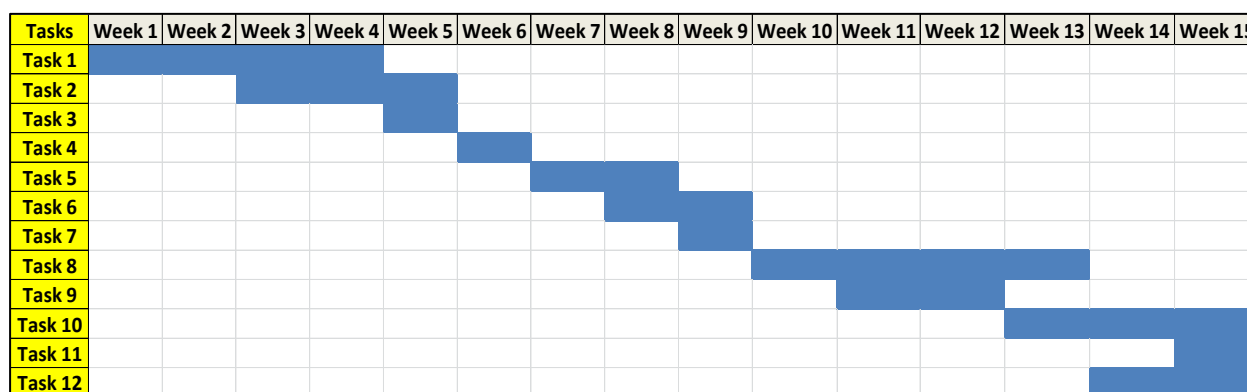


Figure 1-2 Gantt chart summarizing all the tasks done in SDP I.

The main tasks for SDP II are summarized as follows:

- 1) Calibrating the voltage transducer.
- 2) Calibrating the current transducer.
- 3) Studying the different topologies for energy management and selecting one of them to be chosen as a desired scenario for practical implementation.
- 4) Implementing the Maximum Power Point Tracker using Perturb & Observe algorithm.
- 5) Implementing the Energy Management System using different cases.
- 6) Doing the performance assessment.
- 7) Doing the poster.
- 8) Designing the website.

Tasks	Week 1	Week 2	Week 3	Week 4	Week 5	Week 6	Week 7	Week 8	Week 9	Week 10	Week 11	Week 12	Week 13	Week 14
Task 1	█	█	█											
Task 2			█											
Task 3				█	█	█								
Task 4						█	█	█	█	█				
Task 5										█	█	█	█	█
Task 6													█	
Task 7	█													█
Task 8		█												

Figure 1-3 Gantt chart summarizing all the tasks done in SDP II.

Chapter 2 : LITERATURE REVIEW

This chapter presents the solar cars development and evolution of solar car races where the World Solar Challenge is one of the racing competitions aiming to encourage and improve research on sustainable transport with good energy management strategies. The main electrical components of a solar car and the race constraints were also listed and discussed.

Solar cars have actually been built since the 50s; before even establishing the solar car races. Figure 2-1 shows few land marks in the development of solar cars.

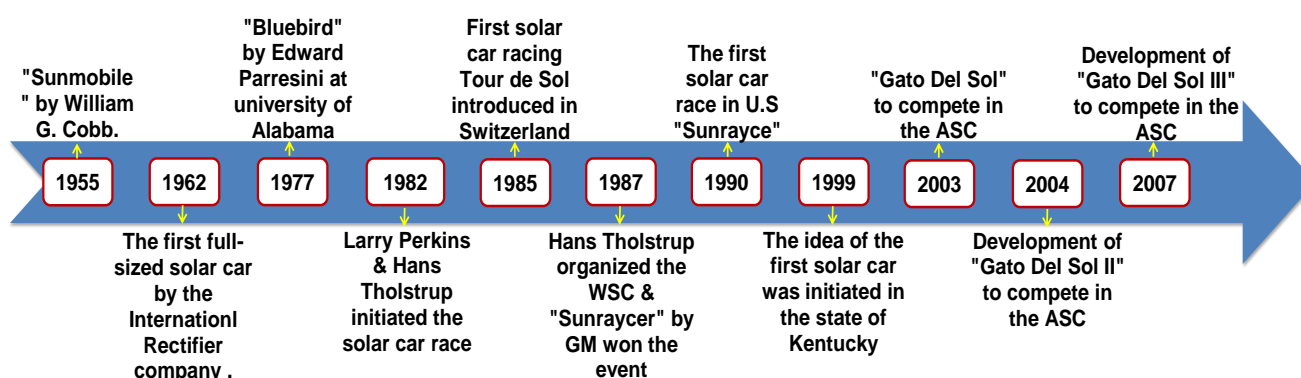


Figure 2-1 Few landmarks in the development of solar cars.

2.1 History of solar cars

The tiny 38 cm vehicle "Sunmobile" shown in Figure 2-2 (a) was the first solar car invented by William G. Cobb of General Motors. On 31st of August 1955, Cobb showcased "Sunmobile" at the Chicago Powerama convention. The car was too small to drive, however it was recognized as the first solar car in the world since "Sunmobile" fulfil the conditions of a solar car, it was made of 12 selenium photovoltaic cells that are connected in a series-parallel configuration to generate electricity that powers a small motor running on 1.5 V to turn the drive shaft and to transfer energy to the wheels causing the car to move forward [5].

The first full-sized solar car that a person could drive was publicized in 1962. The International Rectifier Company improved and modified the Baker electric car shown in Figure 2-2 (b); it is a 50 years old car that was invented in 1912. The company modified the car to run on solar energy via installing photovoltaic panels on the top of the vehicle that contains about 10.640 individual solar cells [5].

After that, the "Bluebird" solar car shown in Figure 2-2 (c) is a prototype full scale vehicle that was built by Professor Edward Passerini at Alabama University in 1977. This solar car was invented to be powered by photovoltaic panels without the back-up battery; it was showcased in the Knoxville but it was not produced massively [5].



(a)

(b)

(c)

Figure 2-2 Development of solar cars: (a) Sunmobile by William G. Cobb; (b) The first full-sized solar car by the International Rectifier Company; (c) Bluebird by Edward Passerini [5].

2.2 Evolution of solar car races

Larry Perkins and Hans Tholstrup initiated the solar car race when they accomplish an impressive Solar Trek from Perth to Sydney in 1982 [6], followed by a consecutive solar car race that aims to raise public attentiveness such as the Tour de Sol that was the first solar car race introduced in 1985 at Switzerland. The first generations achieved average speeds around 60 kmph; however, present generations can attain up to 100 kmph [7]. In 1987, Hans Tholstrup created and organized the world solar challenge (WSC), where 23 participants contributed in the Australian WSC [8], sponsored by South Australia, aiming to validate replacements to conventional vehicle engines and to show the advanced development of automotive technology. Participants in this race involved industry and university research groups around the globe. "Sunracer" by General Motors (GM) shown in Figure 2-3 won the event exceeding 40 kmph [7].



Figure 2-3 Sunracer vehicle by General Motors [9]

After that, in 1990 the first solar car race in the United States named as Sunrayce was established and organized by GM along with the United States Department of Energy (DoE) [7]. Despite of covering the same distance in this race, Sunrayce was more challenging when compared to the WSC, since it was organized in a more diverse and challenging environment [7]. American Solar Challenge (ASC) was the new name of this race in 2001, and then it was renamed as North American Solar Challenge in 2005 [7]. Every two years the race is held with different paths and in 2008 the longest solar vehicle race was recorded for the North American Solar Challenge, by covering 3864 km from Texas, USA to Alberta, Canada [7].

In the state of Kentucky in 1999, the idea of the first solar car was proposed by engineering students. After Sunrayce 99, the publicity of such a racing challenge was tangible among the engineering community [7]. A team of engineers with the solar club started working on building the first solar powered car “Gato Del Sol I” with the help of the UK’s College of Engineering. “Gato Del Sol I” was built by the team to compete in the ASC in 2003, but unfortunately the car was not qualified for the actual race. However, it was a chance to design a better car to race in 2004, and the team was able to secure the second rank in the stock class at the National level Formula Sun Grand Prix. In 2004, the team started developing “Gato Del Sol II” since a more competitive car was required, however, no one can deny that it was a great start to the team [7]. The shell was modified with a rigid fiber glass/polystyrene with extra aerodynamic foil resulting in the reduction of power consumption. Modifying the shell and using lighter chassis reduced 50 % of the weight [7]. From the electrical point of view, lead acid batteries were substituted by nickel metal hydride, and monocrystalline silicon cells replaced polycrystalline silicon cells resulting in a huge power boosting [7]. “Gato Del Sol II” was present at the 2005 North American Solar Challenge, and due to a couple of electrical accidents the car was kept off the road race, nevertheless the insights gained from this experience resulted in the team’s future success. Through the end of 2007, the team continued the work and development process to “Gato Del Sol II”, as the released race rule for the 2008 North American Solar Challenge required remarkable remodel of the car [7]. “Gato Del Sol III” with a 50% new shell, higher capacity lithium polymer batteries, more robust chassis, and more reliable maximum power point trackers secured the 4th place in terms of qualification [7]. The development process of “Gato Del Sol” verified that reliability, powerful solar array, lightweight and aerodynamic design are essential for design teams to build a winning car. It is highly needed to develop a good strategy so that the car sustains in adverse environmental conditions [7].

Table 2-1 Four generations for a sample of a solar car that participated in the ASC [7].

Point of Comparison	Gato Del Sol I (2003)	Gato Del Sol II (2005)	Gato Del Sol III (2008)	Gato Del Sol IV (2010)
Solar Array	Polycrystalline silicon cells	Monocrystalline silicon cells	Monocrystalline silicon cells	Space grade Adv. Triple Junction
Peak Power	800 W	1 kW	1.2 kW	1.5 kW
Weight	449 kg	318 kg	302 kg	272 kg
Shell	Fiberglass	Fiberglass / XEPS foam composite sandwich	Fiberglass / XEPS foam composite sandwich	Carbon fiber / Nomex honeycomb
Motor Drive	DC brushless 9 hp motor			

2.3 World solar challenge

The WSC is a design competition aiming to stimulate and develop research on sustainable transport. Currently, the WSC is the solar car event premiers that attract teams all over the world to race the 3000 km from Darwin to Adelaide [10]. This challenge introduces three distinct classes: Challenger class, Cruiser class, and Adventure class, each with different parameters, stages, and aims [11].

Table 2-2 World Solar Challenge classes [11].

Classes	Challenger	Cruiser	Adventure
Aim	<ul style="list-style-type: none"> ➤ Encounter the requirements for maximizing the solar array. ➤ Meet the driver's vision new requirements. 	<ul style="list-style-type: none"> ➤ Encourages solar cars to be designed practically for the aim of acceptance in a given market segment. 	<ul style="list-style-type: none"> ➤ Allows the previous cars of the event to run again with new members.
Maximum Length	4.5 m	-	5 m
Maximum Width	1.8 m	-	1.8 m
Maximum Solar Array	6 m ²	-	6 m ²
Wheels	4	4	3
Driver	1	1 Driver / 1 Passenger	1
Stages	One single stage from Darwin to Adelaide.	Two stages; Darwin to Alice Springs, and Alice Springs to Adelaide, with an overnight charging stop where teams recharge from the grid.	Two stages; Darwin to Alice Springs, and Alice Springs to Adelaide.

Nowadays, solar cars test the energy efficiency ultimate boundaries and provide visions into the competences of everyday vehicle technology. The following graphs show the average speeds of the winning cars participated in the WSC events that were held from 1987 to 2013 [12].

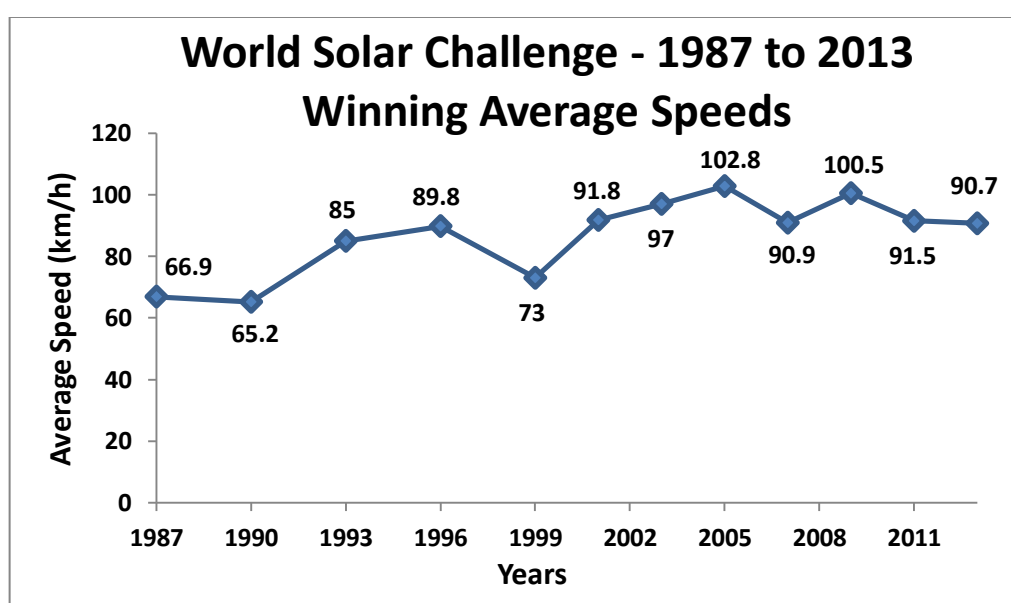


Figure 2-4 Average speeds of the cars participated in the challenger class for previous WSC events.

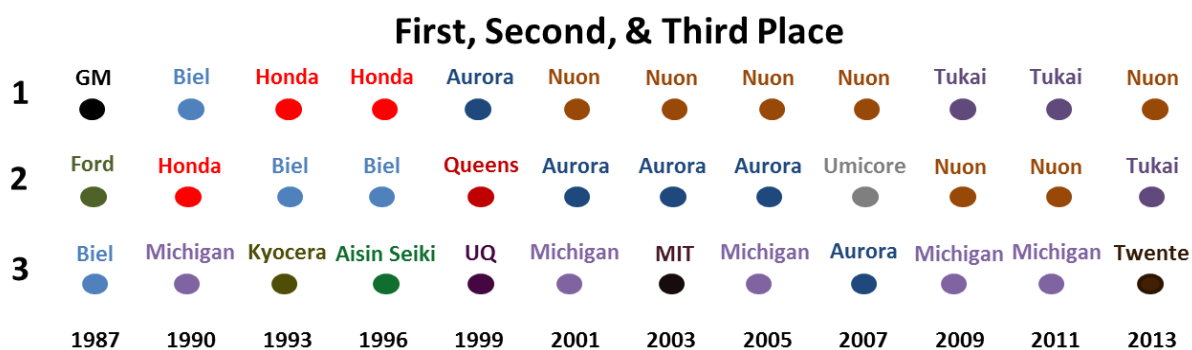


Figure 2-5 The Winning cars in the challenger class for previous WSC events from 1987 to 2013.

2.4 Main components of solar car

A solar car is an electric vehicle powered by energy from the sun via on-board photovoltaic cells that charge the batteries for a more driving extent [3]. The solar car is designed with three main electrical components connected in parallel: the solar panel array, the energy storage system and the electric motor. The storage system can be charged by the array, and both can provide current to the motor [13]. The storage system supplies an energy store for use whenever the solar array is not generating enough energy. Actually, each vehicle is unique, however many common characteristics are shared as some components have few differences, where Table 2-3 shows the basic components of solar cars.

Table 2-3 Basic components of solar car [3].

Electrical Components	Mechanical Components
Photovoltaic cells (Solar arrays)	Exterior lighting
Maximum power point trackers (MPPT)	Body
Energy storage system	Chassis, suspension
Electric drive motor	Tires, and wheels

2.4.1 Solar Arrays:

Photovoltaic cells are constructed of semiconductor materials which can absorb sunlight and convert it to electrical energy. The term itself is derived from the Greek "photo" meaning light, and "voltaic" from Alessandro Volta [8]. The cell is particularly a diode made of crystal silicon [3]. The cell technology selection is a balance of performance, availability, and cost. Solar arrays are built by connecting several individual solar cells in different series and parallel combinations in order to increase the voltage or current output of the array respectively [14].

There are different types of solar panels present in the market nowadays, which are monocrystalline silicon, polycrystalline silicon, and thin film solar panels that include amorphous silicon, cadmium telluride (CdTe) and copper indium gallium selenide (CIS/CIGS), where Table 2-4 shows a comparison between them [15].

Table 2-4 Comparison between the widely used solar cells [15].

Point of Comparison	Monocrystalline	Polycrystalline	Thin film		
			Amorphous	CdTe	CIS/CIGS
Module Efficiency	15-20%	13-16%	6-8%	9-11%	10-12%
Area for 1 kWp	6-9 m ²	8-9 m ²	13-20 m ²	11-13 m ²	9-11 m ²
Warranty	25 years	25 years	10-25 years	-	-
Price	0.75 \$/W	0.62 \$/W	0.69 \$/W	-	-
Temperature Resistance	Performance drops at high temperature.	Less temperature resistant than monocrystalline.	Tolerates extreme heat.	Relatively low impact on performance.	
Further Details	<ul style="list-style-type: none"> ➤ Oldest cell technology and most widely used. ➤ Provides highest output power and space efficient. 	<ul style="list-style-type: none"> ➤ Less silicon waste in the production process. ➤ Lower space efficient compared to monocrystalline. 	<ul style="list-style-type: none"> ➤ Tend to degrade faster than crystalline-based solar panels. ➤ Lower space efficient compared to crystalline-based solar panels. 		

2.4.2 Maximum Power Point Tracker:

The MPPT is basically a DC/DC converter between the solar array and the DC bus as was illustrated in Figure 1-1. The main role of the MPPT is to compensate by regularly selecting an output voltage that delivers the maximum power to the load due to the fact that photovoltaic cells have a single operating point where the values of the current and voltage of the cell yield maximum power output [3]. MPPTs use control logic to look for this point and allow the converter circuit to obtain the maximum power available from a cell [3].

2.4.3 Energy Storage System:

The most common energy storage system used in solar cars is the battery; however, ultra-capacitors are also used when needed in order to provide quick bursts of power. The ultra-capacitors are connected in parallel with the battery pack. Accordingly, adding both storage systems can manage the energy in steady and dynamic states to give the needed current while driving in either normal or accelerating conditions.

A. Battery Pack:

One of the major elements of any electric vehicle is its battery. A battery is an electrochemical energy storage device that can release an electrical charge when needed. It generally consists of an anode, a cathode and an electrolyte (separator) [16]. The battery pack has three main functions: (i) to provide an energy store for use whenever the solar array is not producing enough energy, (ii) to supply direct current to the motor when required, and (iii) to smoothen the fluctuation of the current and voltage output from the PV array into the loads [17]. The solar car battery selection is based on a balanced choice of performance, cost, and safety. Safety is the highest priority in using any battery along with a battery protection system (BPS), which includes battery isolation contactors [3].

Electrical isolation is needed from the battery packs when over-voltage, over-current, under-voltage, or over-temperature conditions take place [3]. The BPS continuously monitors the pack state and takes action in case of a fault, making sure that the system is in a safe condition.

There are four battery choices which are: lithium ion (Li-ion), lithium polymer (Li-Po), lead acid (Pb-Acid), and nickel metal hydride (Ni-MH) [13].

Most of the successful vehicles prefer Li-ion cells because of their superior energy density, or in other words, they provide among the highest energy-to-weight and energy-to-volume ratios [13]. Their charge/discharge efficiency is also high and they have a long life cycle. However, the major disadvantage to this type of cell is that it must be carefully maintained within controlled temperature, voltage, and current. Otherwise, it can fail explosively [13].

The Li-Po battery is similar to other Li-ion batteries except it uses a solid plastic (polymer) electrolyte which means that its cell shape is not limited to the cylindrical or rectangular forms of most others and can be changed to adapt with specific spaces within a vehicle, hence making better use of space. Its other characteristics are similar to Li-ion batteries [16].

The Pb-Acid batteries have high power density but relatively low energy density and they are relatively inexpensive [16]. They are very robust and require only elementary monitoring. On the other hand, the drawback of these cells is that they consume more weight and volume, thus decreasing efficiency by increasing the overall weight, making it harder to design a thin and light car body [13]. Lead acid batteries contain Sulphuric Acid which is corrosive and they emit hydrogen when they are being charged, which is explosive when mixed with air, and can be ignited by a small spark [18].

The Ni-MH batteries have an energy density about twice that of lead-acid batteries and they are moderate in cost, however, their power density is lower in terms of volume. In addition, they have a higher self-discharge rate and therefore tend to discharge when left unused [16].

Table 2-5 2015 World Solar Challenge approved battery chemistry and mass [3].

Battery	Chemistry	Maximum Battery Mass (kg)	Battery Energy Density (Wh/kg)	Battery Energy (Wh)
Lithium-ion	Li-ion	20	160	3200
Lithium-ion polymer	Li-polymer	20	200	4000
Lead-acid	Pb-acid	125	40	5000
Nickel-metal hydride	Ni-MH	70	80	5600
Lithium-iron phosphate	LiFePO ₄	40	90	3600

A battery management system (BMS) acts as a connector between the battery and the vehicle. BMS is essential for improving the performance of the battery and optimizing the operation of the vehicle in a reliable manner [19]. The role of BMS is to ensure safe operation of the battery. To do so, a BMS should be able to monitor and evaluate the state, control the charge, and balance the cells. Since the battery is an electrochemical product that acts differently based on the environmental circumstances, the implementation of these functions is challenging [19].

BMS indicators should express the state of safety, lifetime of the battery, usage, and performance. Due to high temperature a Li-ion battery could ignite if over charged, this could result in a fatal accident, which is really a serious problem especially in vehicles. In addition, over discharge reduces the cell capacity. Thus, BMS should control and observe the battery based on the safe circuitry integrated within the battery packs. Such that, whenever there is any abnormal situations like over heating or over voltage are monitored, the BMS should inform the user [19]. A BMS should also observe the temperature of the system in order to deliver an improved power consumption scheme. Therefore, a comprehensive BMS should include the following functions [19].

1. Data acquisition
2. Cell balancing and Thermal management
3. Safety protection
4. Delivery of battery status to a user interface
5. Ability to determine the state of the battery
6. Communication with all battery components
7. Ability to control battery charging and discharging
8. Prolonged battery life

The mentioned functions could be combined into a generic BMS structure as shown in Figure 2-6 [19].

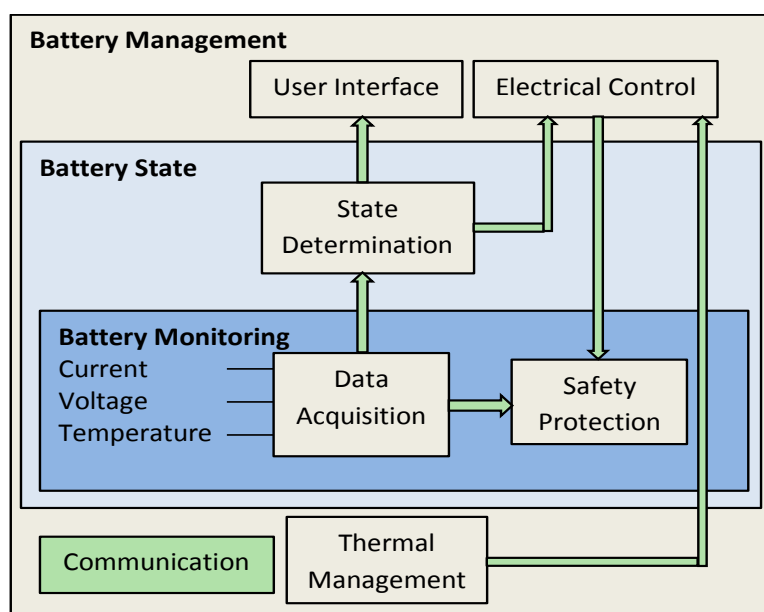


Figure 2-6 Battery Management System.

Knowing the state of the battery not only determines whether the operational environment is safe and reliable, but also gives information about the charge and discharge operation, which is significant for cell balancing. The state of the battery usually includes state of charge (SoC) and state of health (SoH) determination. SoC reflects the amount of charge remaining and is available to the battery. However, SoH reflects the health condition of the battery and its ability to perform when compared to a fresh battery. A BMS could also include state of life (SoL) determination that refers to the useful life remaining in a battery, or in other words, SoL reflects the time where the battery should be replaced. Battery performance prediction helps engineers to handle disposals and issues [19].

In a battery pack, cells are wired in parallel to provide high capacity, and connected in series to provide high voltage. Each cell is distinct from the other due to chemical offset and manufacturing. Thus an effective cell balancing mechanism that keeps the SoC of individual cells close to each other should be developed, to maintain the battery lifetime. To further illustrate, cells charging and discharging at different levels will affect the battery's lifetime [19].

B. Ultra-capacitors

Ultra-capacitors serve as temporary energy storage that can store and discharge energy very quickly and efficiently. Ultra-capacitors complement a primary energy source which cannot repeatedly supply quick bursts of power, such as battery or fuel cell [20].

Table 2-6 Comparison between batteries and ultra-capacitors.

Type of Energy Storage	Description	
Batteries	Batteries operate well as a continuous source of low power. However, they cannot handle peak power demands since they discharge and recharge slowly.	
Ultra-capacitors	Ultra-capacitors deliver quick amount of energy during peak power demands, then store energy and capture excess power quickly that is otherwise lost. They complement a primary energy source since they discharge and recharge quickly.	

2.4.4 Electric Motor:

Solar cars usually use a three-phase brushless DC (BLDC) permanent magnet motor to convert the electrical energy into mechanical torque [7]. The BLDC motor is alternating current electric motor excited by DC electricity and from a mathematical modeling viewpoint looks similar to DC motors [3]. The axial flux BLDC named as “pancake” has a stationary, wound stator and two rings of magnets that turns the wheel and makes the car moves [3]. Power converter controls the motor through pulse width modulation (PWM) [7].

While racing, the power stored in the batteries and the instantaneous power from the solar cells is used through the converter to power the efficient electric motor. The power converter turns the DC into a three phase AC capable of running the motor [21]. It tracks the relative position of the rotor and stator, such that the proper phase is applied to the correct winding in the motor at the right time [21]. Hence, the power converter manages the desired motor power.

The motor can also be used to generate electricity. Most motor controllers allow the driver to brake using the motor instead of mechanical brakes where the motor is turned into a generator and energy flows backwards through the motor controller and into the batteries for storage [13]. This is called regenerative braking because it allows the substantial forces in the process of braking to be converted

back into electrical energy to be used in recharging the batteries [13]. The amount of energy returned to the batteries is small, but every bit helps to improve the car efficiency.

2.5 Constraints

Building an efficient "winning" vehicle is the main goal of any solar car manufacturer [8]. Design constraints include hundreds of trade-offs, however, certain elements are fundamental [8]. Students must design their car considering reliability to be competitive in such event. It must operate effectively for hundreds of hours under harsh environmental conditions along with many other systems and components [13]. Safety is the most significant design constraint, since the vehicle is driven by students. All failure modes should be carefully considered, and defensive mechanisms should be designed into every safety critical system [13]. A main factor for success is vehicle efficiency, which requires a well thought-out system. Another important design issue is the solar car overall shape. Teams have to identify how they would mount the solar cells for maximum energy. They also must decide how to minimize aerodynamic drag and maintain low weight. A typical solar car produces 700-1500 watts of power from PV [8]. This makes aerodynamic drag and rolling friction essential concerns [8]. Battery management is actually significant due to the fact that a dead or badly depleted battery is the extreme failure in solar car racing. With an exhausted battery, a team has no choice other than slowing down to let the solar array recharge it. The process could take hours, which can lead the team to simply lose a hundred kilometres to other challengers [21].

Any participating car must meet the standards and design criteria described by the regulations of the WSC competition, which are as follows [22]:

- The Challenger Class Solar EV dimensions must not exceed 4.5 m in length, 1.8 m in width and 2.2 m in height.
- The Challenger Class Solar EV configuration must have four wheels: two front wheels and two back wheels.
- All front tyres must be of the same type and all back tyres must be of the same type.
- The driver's eyes must be not less than 0.7 m above the road when seated in a normal driving position. The Challenger Class Solar EV driver must be able to see every point between 0.4 m and 0.7 m below and above eye level respectively at a distance of 4 m from the driver's eyes, at every forward angle. The Solar EV must have back vision systems that allow the driver to see backwards from the normal driving position with the fastened seatbelt either electronic, mirrors, or both.
- A minimum of two drivers and a maximum of four drivers must be available for every vehicle associated with the team where only registered Solar EV drivers may drive the Solar EV during event hours.
- Team drivers must demonstrate that they can exit the Solar EV in less than 15 seconds without assistance. The Challenger Class Solar EV must have access points or doors that are protected and released from both inside and outside the Solar EV.

- The Solar EV must have two independent mechanical braking systems, so that if one system fails the other can stop the Solar EV and they must be applied to at least two wheels.
- The steering system must have minimal backlash, and be designed with sufficient strength and stiffness to guarantee better driving control in all conditions.
- The only external energy source that may be used by the Challenger Class Solar EV is the solar irradiation received directly by the Solar EV where photovoltaic cells acceptable area is:
 - Not more than 6 m² for Solar EVs using only silicon photovoltaic cells.
 - Not more than 3 m² for Solar EVs using only GaAs photovoltaic cells.
- The sum of the nominal cell masses for the electrochemical battery used as an energy storage system for the Challenger Class Solar EV may not exceed the following limits:

Table 2-7 Battery weight limitations.

Li-ion	Li-Polymer	LiFePO4	Ni-MH	Pb-Acid
20kg	20 kg	40 kg	70 kg	125 kg

- The allowed total energy capacity of cells must not exceed 2 Wh.
- The energy storage system must not be more than two packs.
- Capacitors with total energy storage capacity less than 10 Wh are not considered to be part of the energy storage system.
- The Solar EV must have a designed battery monitoring system to detect overcharged, undercharged, or too hot component cell. However, other types of energy storage system must have equivalent designed safety systems to avoid the uncontrolled release of energy.

Chapter 3 : PV & MAXIMUM POWER POINT TRACKING

In this chapter, PV modeling is simulated using Matlab/Simulink with the help of SimPowerSystem toolbox. In addition, MPPT is discussed using the P&O technique because of the PV non-linear I-V characteristics.

3.1 PV Modeling

PV systems are used in distributed power generation systems. In addition, it could be used as a standalone system [14]. Due to the change in environmental conditions, a PV array fails to operate at the maximum power point (MPP), hence the efficiency of the PV array decreases. Consequently, PV modeling has attracted the researchers' attention to ease modeling the PV-based power systems dynamic performance [14]. The PV system modeling is very critical for embedded power system applications and maximum power point tracking [14]. In this section, the performance of the PV array is simulated and monitored using the PV cell. The PV model has been developed and used as Simulink subsystems where the simulated I-V and P-V output characteristics shows the solar insolation and PV array temperature effect on commercial PV modules.

3.1.1 PV Hierarchy:

- **PV Cell:** Is a semiconductor p-n junction-based photodiode that generates electrical power when exposed to light. Various semiconductor materials can be used to make PV cells; however, monocrystalline silicon and polycrystalline silicon are the most common commercial types [14].
- **PV Module:** Usually, PV cells are connected in series and in parallel configurations to obtain higher voltage and higher current respectively; hence, higher power. This is done due to the fact that a single PV cell cannot produce enough power. A module is a combination of series and parallel connection that mostly consists of 36 or 72 cells. The modules are made of transparent front side, encapsulated PV cells, and back side, where low-iron and tempered glass are usually the materials that the front side is made of. Due to the fact that some solar irradiation is reflected by the glass cover and frame shadowing, the efficiency of a PV module is less than a PV cell [14].
- **PV Array:** Is an interconnection of modules which consists of many PV cells connected in series and parallel. Modules are connected to form an array in order to supply the load since the power produced by a single module is not enough for commercial use. The modules' connection to form an array is similar to the cells' connection to form a module. A string is formed when several modules are connected in series, while an array is formed when several strings are connected in parallel [14].

3.1.2 PV Cell Model:

Observing and evaluating the PV behaviour and discovering different PV MPPT approaches are the main reasons for using the equivalent circuit-based model [14].

PV cell can be modelled using the:

- **General Model:** Figure 3-1 shows the general model equivalent circuit of a PV cell, where the components of a PV cell are: photo current source, diode, parallel resistor reflecting the leakage current, and series resistor expressing the internal resistance to the current flow [14]. The PV cell I-V characteristic equation is given as:

$$I = I_{PH} - I_S \left(\exp \left[\frac{q(V + IR_S)}{kTA} \right] - 1 \right) - \frac{(V + IR_S)}{R_{SH}}$$

Where;

I_{PH} : Light-generated current or photocurrent.

I_S : Cell saturation of dark current.

q : Electron charge ($=1.6 \times 10^{-19}$ C).

k : Boltzmann constant ($= 1.38 \times 10^{-23}$ J/K).

T : Cell working temperature.

A : Ideal factor (dependent on PV technology).

R_{SH} : Shunt resistance.

R_S : Series resistance.

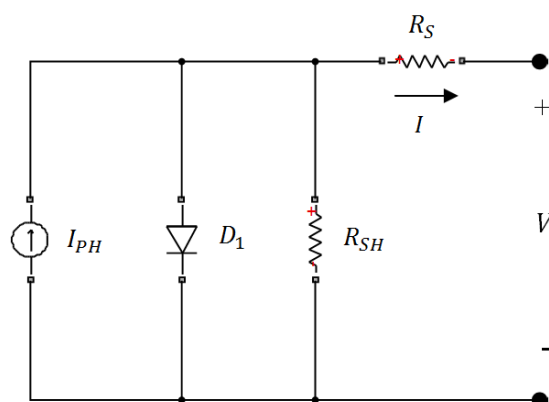


Figure 3-1 Equivalent circuit of a PV cell.

Solar insolation and cell working temperature are the main factors that the photocurrent depends on, given as:

$$I_{PH} = \lambda(I_{SC} + K_I(T - T_r))$$

Where;

I_{SC} : Cell short-circuit current at 25 °C and 1 kW/m².

K_I : Cell short-circuit current temperature coefficient.

T_r : Cell reference temperature.

λ : Solar insolation in kW/m².

However, the cell saturation current depends on the cell temperature, given as:

$$I_S = I_{RS} \left(\frac{T}{T_r} \right)^3 \exp \left[q E_G \frac{\left(\frac{1}{T_r} - \frac{1}{T} \right)}{kA} \right]$$

Where;

I_{RS} : Cell reverse saturation current at a reference temperature and a solar radiation.

E_G : Band-gap energy of the semiconductor used in the cell.

The reverse saturation current at reference temperature can be approximately found as:

$$I_{RS} = \frac{I_{SC}}{\exp \left[\frac{qV_{OC}}{N_S kAT} \right] - 1}$$

Where;

V_{OC} : PV open-circuit voltage at the reference temperature.

- **Double Exponential Model:** Another accurate model describing the PV cell is the double exponential model; resulted and derived from the PV cell physical behaviour made-up from polycrystalline silicon [14]. Light-generated current source, two diodes, a series resistance and a parallel resistance are the components of this model. This model is narrowly used and not considered for the generalized PV model since the I-V curve parameters expressions are difficult to develop due to the implicit and nonlinear behaviour of the model [14].
- **Approximate Model:** Deriving the PV cell approximate model with proper intricacy from Eq. (1) by ignoring the shunt resistance effect [14], can be modified as:

$$I = I_{PH} - I_S \left(\exp \left[\frac{q(V + IR_S)}{kTA} \right] - 1 \right) - \frac{(V + IR_S)}{R_{SH}}$$

- **Simplified Model:** Ideally, a PV cell has no series loss ($R_S = 0$) and no leakage to ground ($R_{SH} = \infty$) [14]. The PV cell equivalent circuit is simplified by modifying Eq. (1) as:

$$I = I_{PH} - I_S \left(\exp \left[\frac{qV}{kTA} \right] - 1 \right)$$

3.1.3 PV Module & PV Array Model:

As previously mentioned, in order to produce sufficient power, cells should be set in series-parallel configuration on a module to generate the required current and voltage; due to the fact that a PV cell produces insufficient power [14]. Figure 3-2 shows the equivalent circuit for a PV module arranged in N_P parallel and N_S series cells, where the terminal equation for the current and voltage of the array is:

$$I = N_P I_{PH} - N_P I_S \left(\exp \left[\frac{q \left(\frac{V}{N_S} + \frac{IR_S}{N_P} \right)}{kTA} \right] - 1 \right) - \frac{\left(\frac{N_P V}{N_S} + IR_S \right)}{R_{SH}}$$

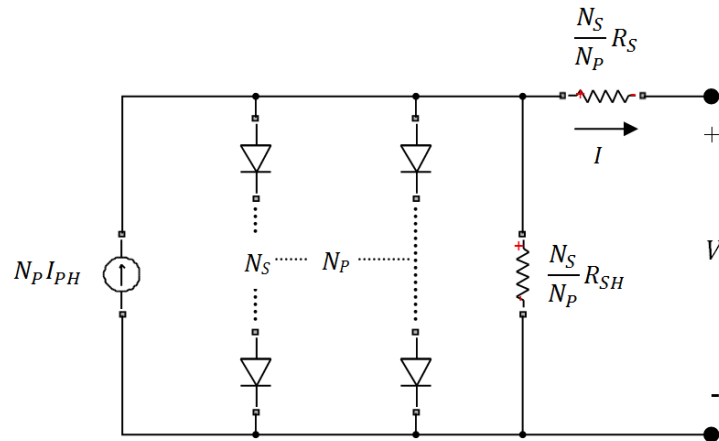


Figure 3-2 Generalized array model.

Figure 3-3 shows the PV cell, module, and array approximate equivalent circuit, where the current can be expressed as:

$$I = N_P I_{PH} - N_P I_S \left(\exp \left[\frac{q \left(\frac{V}{N_S} + \frac{I R_S}{N_P} \right)}{k T A} \right] - 1 \right)$$

Where;

$N_S = N_P = 1$ for a PV cell, N_S and N_P are the series-parallel number for a PV array.

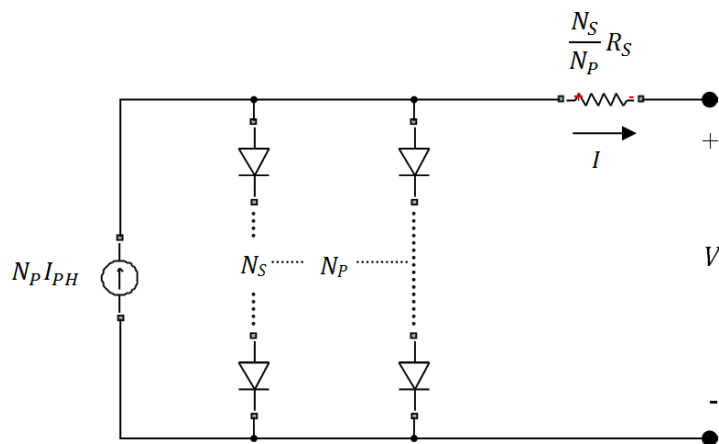


Figure 3-3 Approximate array model.

Figure 3-4 illustrates a generalized PV array simplified model, where the equivalent circuit is described as:

$$I = N_P I_{PH} - N_P I_S \left(\exp \left[\frac{q V}{N_S k T A} \right] - 1 \right)$$

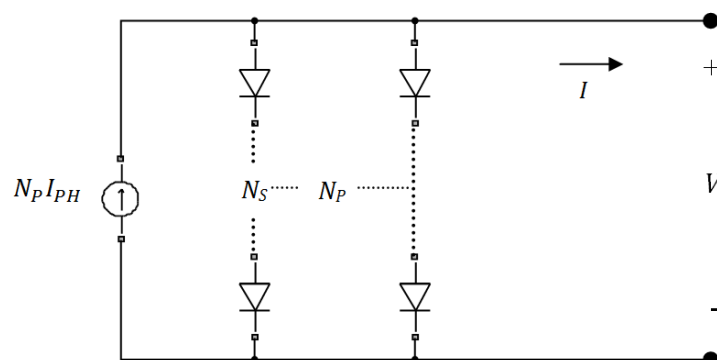


Figure 3-4 Simplified array model.

3.1.4 Mathematical Models of PV Module & PV Array:

Matlab/Simulink has been used for PV modeling using the simplified PV module and array models. Experiencing algebraic loop problems with the other two models using Matlab/Simulink simulation is the main reason for choosing the simplified PV model [14]. To further illustrate, the output current is required to be an input to the equations of output current in the other two models, in which iterations may be required for solving this issue; however this results in a simulation break in many cases [14].

To monitor and assess the PV module/array nonlinear I-V and P-V output characteristics, the mathematical modeling and the physical modeling can be used to simulate the PV module model. However, it was decided to use the mathematical model due to the fact that the mathematical model has more advantages than the physical model; since additional parameters as: quality factor and semi-conductor band gap energy can be varied [14]. In addition, block diagrams are not repeated to form parallel and series PV cells configurations, unlike the physical model where the block of the PV cell should be replicated when forming a parallel combination, consequently the model will be more complicated [14].

Figure B-1 in Appendix B shows the detailed mathematically modelled simplified PV module. However, Figure 3-5 shows the same model after creating the subsystem and Figure 3-6 shows the Simulink model illustrating the I-V and P-V output characteristics. The PV array Simulink model is achieved by adding the gain blocks as shown in Figure 3-7.

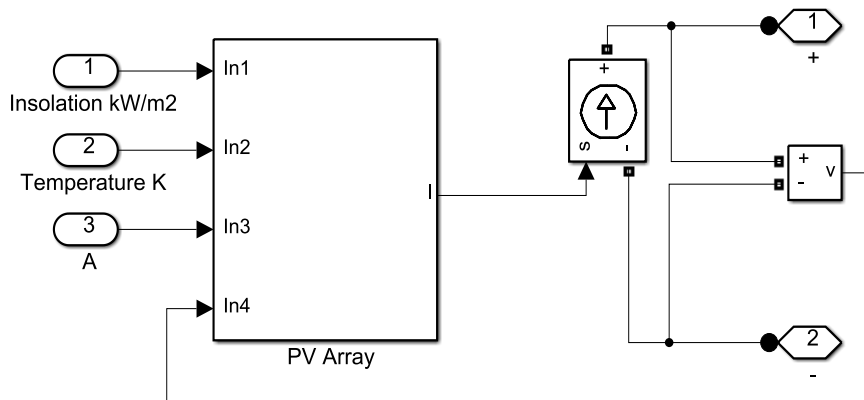


Figure 3-5 Mathematically modelled PV module interfaced to the physical ports.

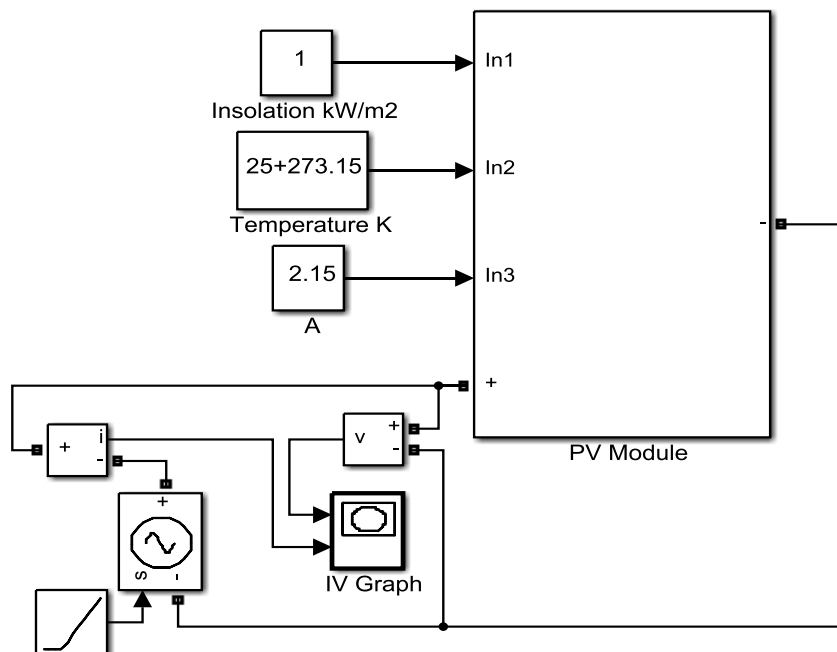


Figure 3-6 Simulink model of a PV module illustrating the I-V and P-V output characteristics.

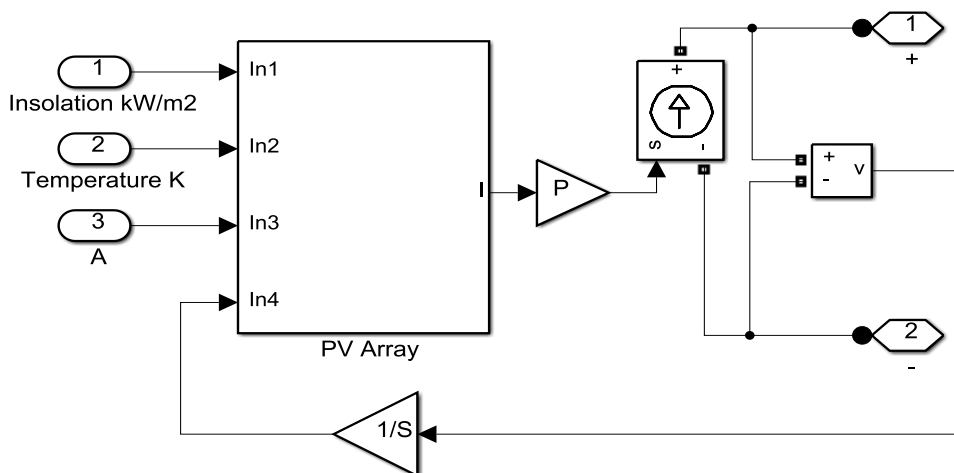


Figure 3-7 Mathematically modelled PV array interfaced to the physical ports.

3.1.5 Results and Discussion:

The I-V and P-V characteristics of the Solarex MSX 60 PV module are simulated and studied, where the specifications of the module are listed in Table 3-1. First, the operating temperature was varied at constant insolation, after that the solar insolation was varied at a constant temperature level to study the PV module I-V and P-V characteristics. The operating temperature and insolation level are varied taking into consideration the race conditions. In other words, the range where the model is tested includes the expected race conditions during the competition.

Table 3-1 Solarex MSX 60 PV module specifications at 1 kW/m² and 25 °C [14].

Characteristic	Specification
Typical peak power	60 W
Voltage at peak power	17.1 V
Current at peak power	3.5 A
Short-circuit current	3.8 A
Open-circuit voltage	21.1 V
Temperature coefficient of open-circuit voltage	-73 mV/°C
Temperature coefficient of short-circuit current	3 mA/°C
Approximate effect of temperature on power	-0.38 W/°C
Number of series cells in the array	36

➤ **I-V and P-V characteristics with varying Solar Insolation Level:**

It is observed from Figure 3-8 and Figure 3-9 that when the solar insolation increases, the PV module short-circuit current as well as the maximum power output increases.

➤ **I-V and P-V characteristics with varying Operating Temperature:**

It is noticed from Figure 3-10 and Figure 3-11 that when the operating temperature increases, the PV module open-circuit voltage as well as the maximum power output decreases.

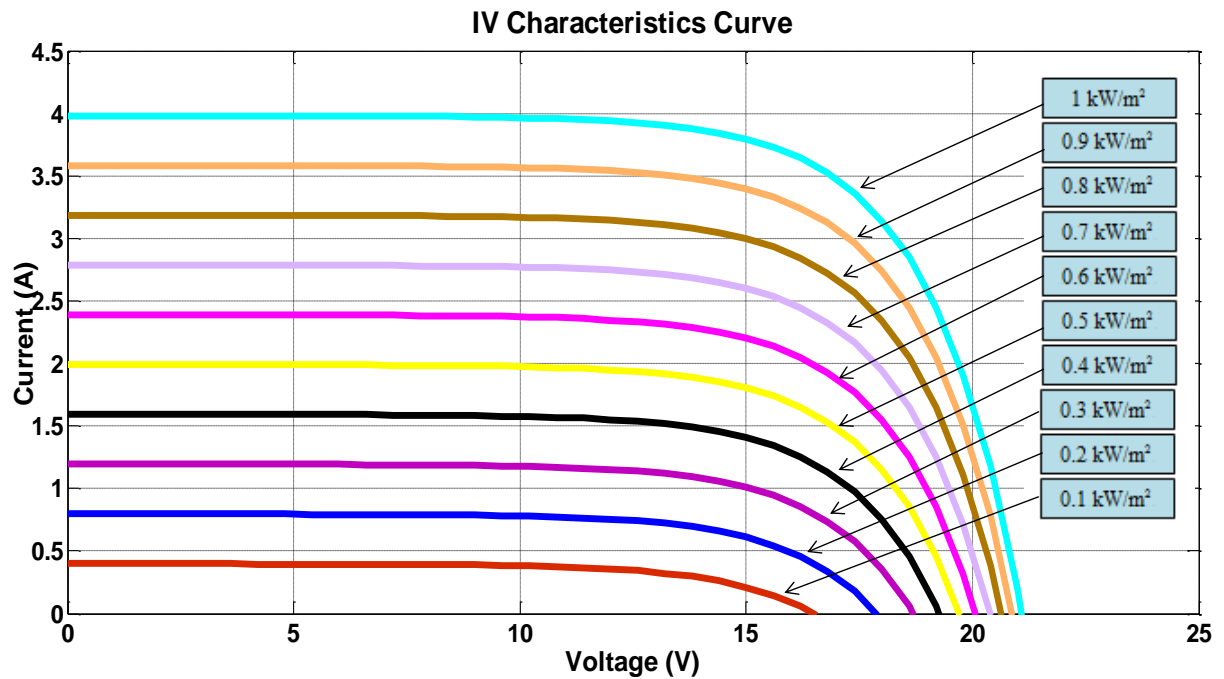


Figure 3-8 I-V output characteristics with different values of solar insolation at constant temperature level of 25°C.

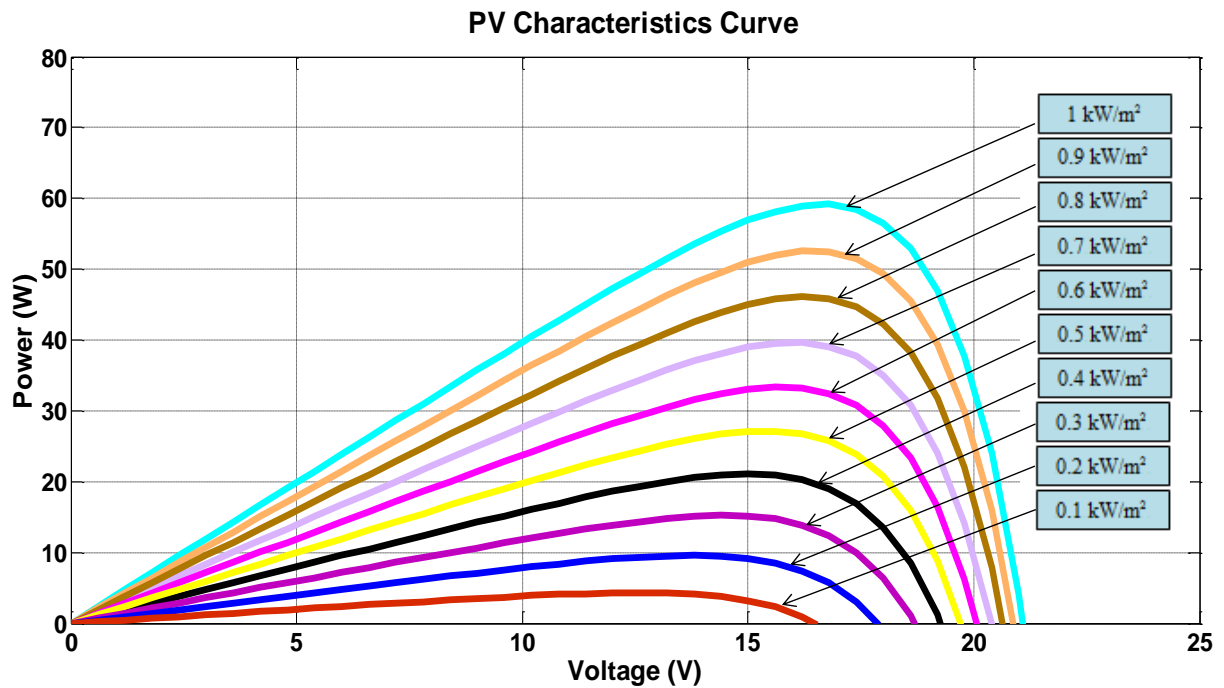


Figure 3-9 P-V output characteristics with different values of solar insolation at constant temperature level of 25°C.

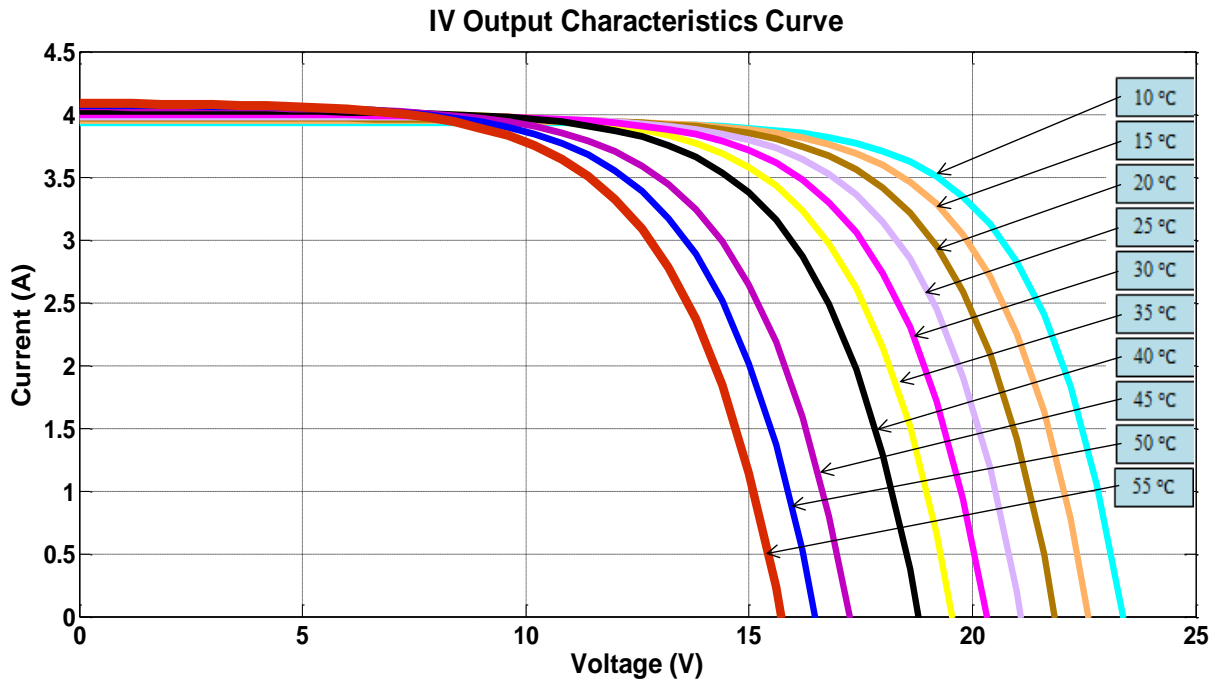


Figure 3-10 I-V output characteristics with different values of operating temperature at constant insolation level of 1kW/m^2 .

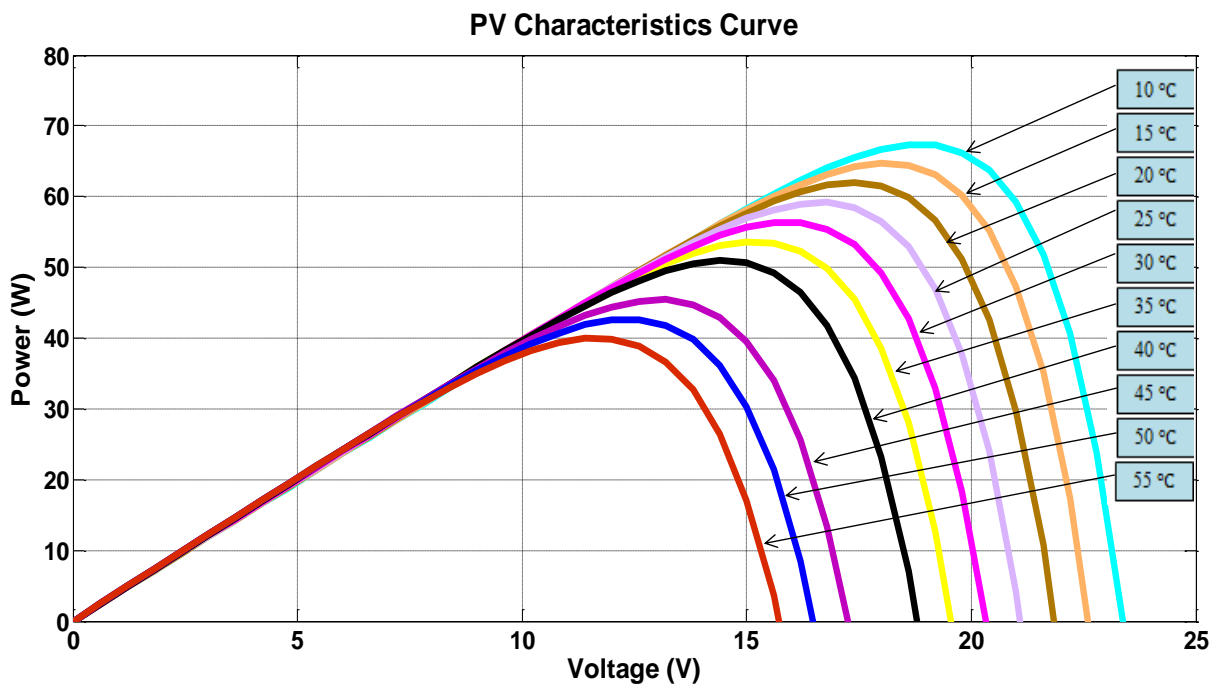


Figure 3-11 P-V output characteristics with different values of operating temperature at constant insolation level of 1kW/m^2 .

3.2 MPPT Modelling using Perturb and Observe Technique

Due to the PV non-linear I-V characteristics affected by the temperature and irradiance level, PV panels do not operate continuously at maximum power point. Consequently, Maximum Power Point Trackers (MPPTs) are added to keep the PV system operating at the optimum point which is the knee of the I-V curve to deliver the maximum power [23]. Figure 3-12 illustrates the PV conversion system that maximizes the power drawn from the PV panel, where the PV array is connected to the battery through a DC/DC converter. The battery is used at the output side of the converter to fix the converter output voltage. As a result, by adjusting the duty cycle of the converter and fixing the output of the DC/DC converter, the voltage of the PV array can be changed to reach the MPP. There are different techniques that are used to track the maximum power point (MPP). One of the widely used techniques is the perturb and observe (P&O) method; due to the fact that it is low in cost, simple in algorithm, good in performance, and easy to implement [24] [25].

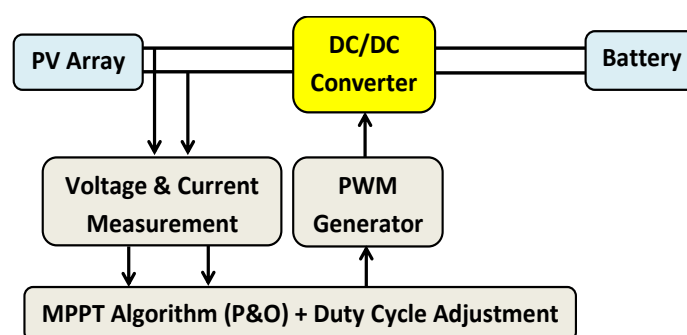


Figure 3-12 PV conversion system.

3.2.1 P&O Algorithm:

In the P&O algorithm, perturbation is provided to the PV module/array voltage which would translate to an increase or decrease in power as shown in Figure 3-13. If an increase in the PV array operating voltage leads to an increase in the power drawn from the PV array, this means that the operating point is to the left of the MPP and is moving toward the MPP [25]. Therefore, the voltage must be further increased to reach the MPP. In other words, the PV array voltage must be further perturbed in the same direction. However, if this increase in the PV array operating voltage leads to a decrease in the power drawn from the PV array, this means that the operating point is to the right of the MPP and is moving away from the MPP [25]. Therefore, the voltage must be decreased to reach the MPP. In other words, the voltage perturbation direction should be reversed. Accordingly, P&O is based on varying the output voltage of the PV module/array, adjusting DC/DC converter duty cycle, and comparing the power drawn from the PV array at the current instant of time with the power drawn at the previous instant of time [25]. Figure 3-14 shows the flow chart of P&O algorithm.

P&O technique suffers several demerits. First of all, the oscillations of the operating point around the MPP at steady state results in wasting the amount of available energy. As a result, improvements have been proposed to decrease the number of oscillations around the MPP at steady state. However, these enhancements slow down the algorithm response, lowering its efficiency [26]. Hence, there is a trade-off problem between faster response and steady-state oscillations [24]. In addition, Qatar University First Solar Car to Compete in the World Solar Challenge: Design of Energy Management System

P&O method fails to track the MPP through the time intervals characterized by varying atmospheric circumstances, since the operating point moves away from the MPP during these intervals.

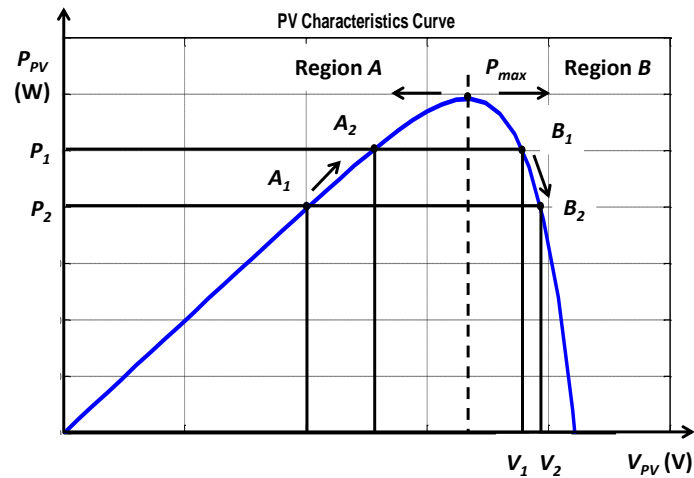


Figure 3-13 P&O algorithm.

3.2.2 P&O Flowchart:

The P&O algorithm is shown as a flow chart illustrating four different cases, and depending on the current situation, an action will be taken to change and adjust the duty cycle of the converter using a fixed perturbation size, so that PV module voltage is changed and the maximum power is drawn from the PV module.

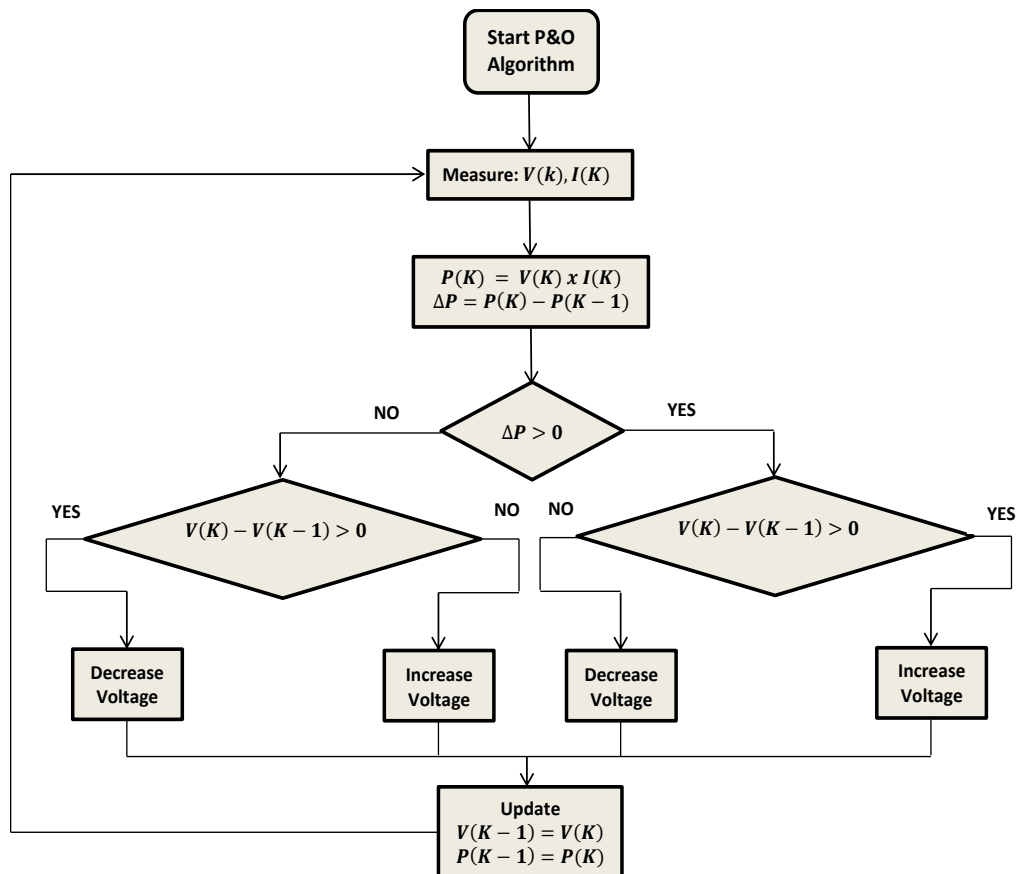


Figure 3-14 P&O flowchart [27].

3.2.3 Model of MPPT:

In this section, P&O technique is used with the PV module modeled in section 3.1 to track the maximum power point. To further illustrate, the P&O flowchart shown in Figure 3-14 was developed using an embedded Matlab function block to update the voltage and power values by adjusting the duty cycle of the power converter that will be used to increase or decrease the output voltage of the PV so that it matches the DC bus voltage. To further illustrate, perturbation to the output voltage of the PV is done by using a fixed perturbation size that will change the duty cycle continuously and accordingly the PV voltage will change since the output voltage of the converter is fixed. As shown in Figure B-2 in Appendix B, the model is developed by sensing the voltage and current of the PV and based on the values the duty cycle will be adjusted by a certain step size so that the PV will always operate at the MPP.

According to the Solarex MSX 60 PV module specifications at 1 kW/m^2 and 25°C listed in Table 3-1, now as shown in the following figure, the PV is operating at the MPP, where the current, voltage, and power values are 3.5 A, 17 V, 60 W respectively.

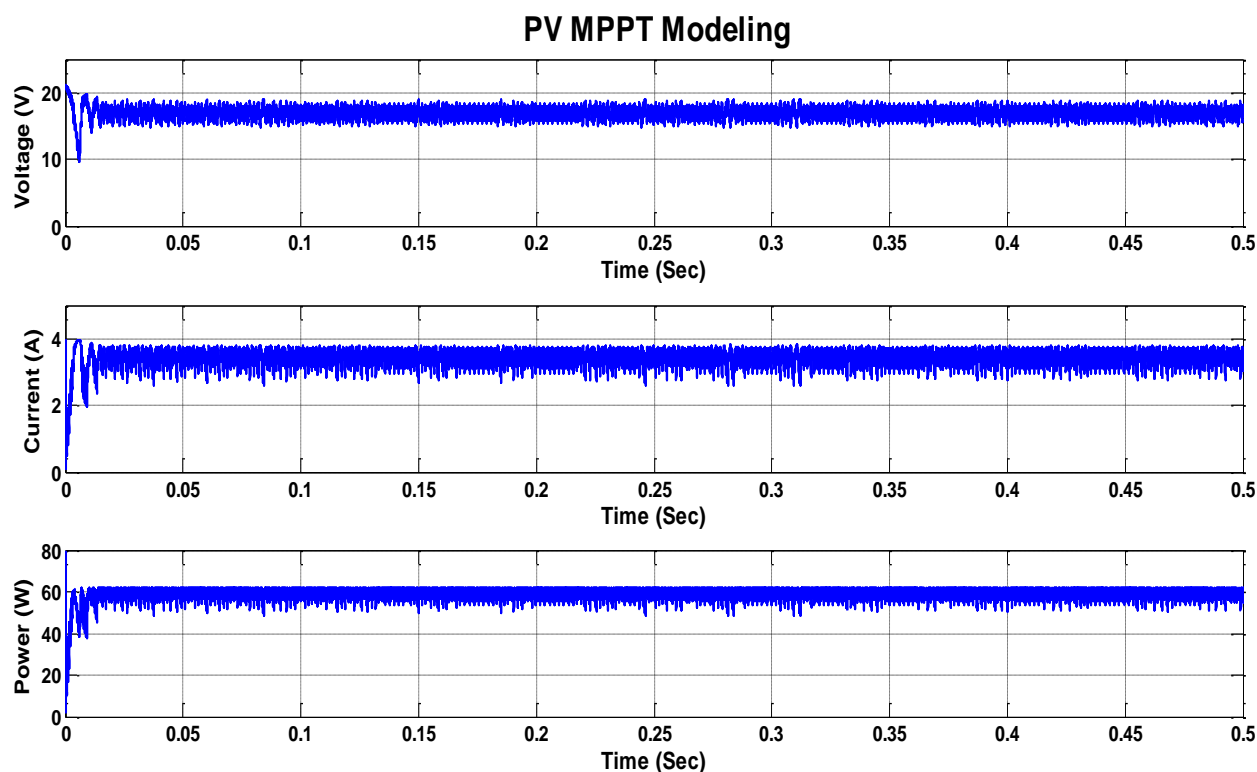


Figure 3-15 PV module voltage, current, and power curves at insolation level of 1 kW/m^2 and temperature level of 25°C .

Chapter 4 : DESIGN OF SOLAR CAR ELECTRICAL SYSTEM

This chapter presents the selection and the design of the electrical components for the solar car in order to achieve the maximum efficiency. Although the MPPT is a part of the electrical system, it is discussed in another chapter because of its importance and relation to the PV.

4.1 Solar Panel

Silicon used in PV panels has different forms; the silicon purity, which is how the silicon molecules are aligned, is the main difference. The solar cell will convert solar energy to electric energy in a better way, resulting in higher efficiency as long as the silicon molecules are perfectly aligned [28]. However, the enhancement processes of the silicon purity are expensive [28]. Space efficiency and cost are also determining factors that should be taken into consideration.

All of the PV panels will be connected in parallel to overcome the shading problem. It is decided to choose **Monocrystalline** (single crystalline) silicon solar panels due to the following reasons [28]:

- They have the highest efficiency rates since they are made of the highest-grade silicon. As mentioned in Table 2-4 the efficiency of such panels is typically 15% - 20%. However SunPower manufacturer produces the highest solar panel efficiency. For instance, E20 series and the X series provide panel conversion efficiency up to 20.1 % and 21.5 % respectively. Table 4-1 shows the X series solar panel specifications.
- They are space efficient, since they require the least amount of space when compared to other types. In addition, they produce the highest power outputs.
- They have long lifetime that is why most of the solar panel manufacturers set 25 years as guarantee on the monocrystalline solar panels.
- Perform better than polycrystalline solar panels in low light conditions.

The simulated PV model is not X series solar panel; however, it has the same behaviour of the simulated PV panel in chapter 3 but with a different scaling factor.

Table 4-1 X series solar panel specifications.

Characteristic	Specification
Nominal Power P_{nom}	345 W
Avg. Panel Efficiency	21.5 %
Rated Voltage V_{mpp}	57.3 V
Rated Current I_{mpp}	6.02 A
Open-Circuit Voltage V_{OC}	68.2 V
Short-Circuit Current I_{SC}	6.39 A
Power Temp. Coefficient P_{mpp}	-0.30 %/°C
Voltage Temp. Coefficient V_{OC}	-167.4 mV/°C
Current Temp. Coefficient I_{SC}	3.5 mA/°C

4.2 Battery Pack

Lithium ion (Li-Ion) battery is the ideal choice to be used for the solar car because of the following reasons:

- High energy density.
- Fast & efficient charging.
- Relatively low self-discharge.
- Extended cycle life.
- Size & Weight advantages.
- Low maintenance.

According to previous teams' experience, a typical lithium ion battery has a minimum power density of 100 Wh/kg, and rated power of 250 W/kg.

4.3 DC/DC Converters

DC conversion usage has expanded in numerous applications, starting from low power applications to high power applications. DC/DC converters are power electronic circuits that convert an unregulated DC voltage input into a regulated output voltage with different voltage level, it is considered as a DC transformer that provides a lossless energy transfer at different levels of voltage [29]. Electronic, magnetic, capacitive, linear, and switched mode are different topologies of conversion method [30]. The circuits described in this report are classified as switched mode DC/DC converters. Figure 4-1 illustrates the five non-isolated switched mode DC/DC converters, however, it can be considered that the basic DC/DC converters are: Buck, Boost, and Buck-Boost, since Cuk and SEPIC can be replaced by Buck-Boost converter.

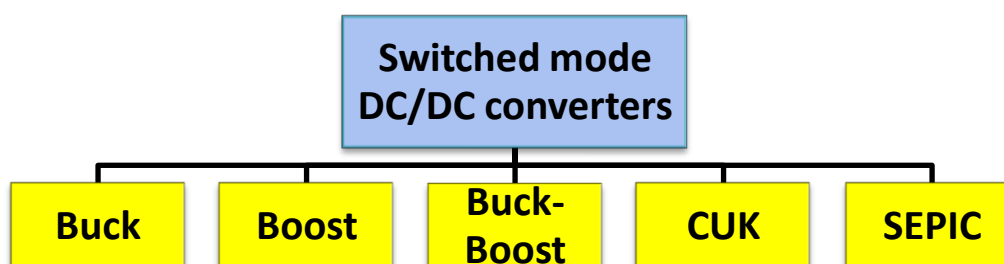


Figure 4-1 Switched mode DC/DC converters.

The Buck Converter shown in Figure 4-2 produces a regulated DC output voltage that is lower than the unregulated DC input voltage [30]. However, the Boost Converter shown in Figure 4-2 produces a regulated DC output voltage that is higher than the unregulated DC input voltage [30]. A combination of the previous two DC/DC converters results in a Buck-Boost Converter shown in Figure 4-4, it produces a regulated DC output voltage that is either higher or lower than the unregulated DC input voltage [30] and has the characteristics of Buck and Boost converters [31].

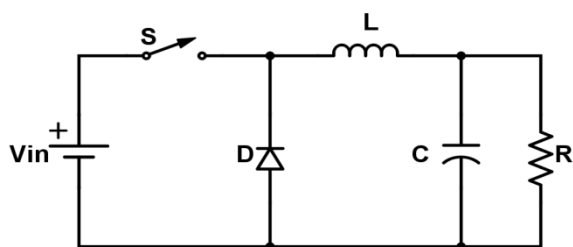


Figure 4-2 Buck Converter.

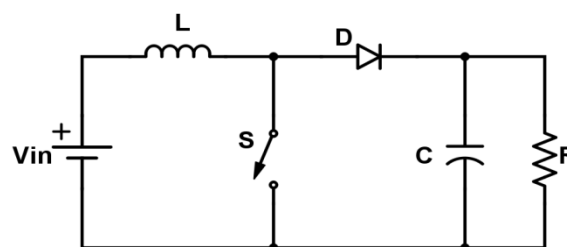


Figure 4-3 Boost Converter.

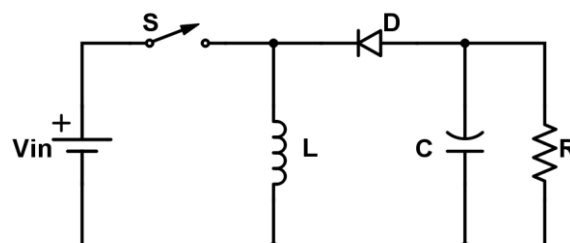


Figure 4-4 Buck-Boost Converter.

Bidirectional DC/DC converters accompanied with the energy storage device have become a promising alternative for many power systems, including hybrid vehicles, electric vehicles, and of course solar powered vehicles, since it reduces the cost and improves the system efficiency [32]. Adjusting voltage and current levels and controlling the energy between the storage elements and the motor, is recognized via DC/DC power converters. These power converters allow the control of power flow to or from each storage device according to the power demand of the load. In other words, DC/DC converters designed for both energy storage devices (battery and ultra-capacitors) will control the flow direction of power according to the load requirements. In this project, bidirectional converters are highly needed for the two energy storage devices to absorb the regenerated energy, which is fed back by the BLDC motor [32]. In addition, such converter is needed to draw power from the battery to boost or buck the voltage according to the bus voltage during vehicle starting, acceleration and hill climbing [32]. Since bidirectional DC/DC converters have the ability to reverse the direction of the current flow and thereby power, they are used to achieve power transfer between the energy storage devices and the motor in either direction [32]. To further illustrate, bidirectional DC/DC converters means that the power can flow in both directions from the storage device to the load (motor) which means that the battery/ultra-capacitors are discharging and from the load to the energy storage device which means that the battery/ultra-capacitors are charging. However, the DC/DC converter designed for the PV modules is a unidirectional DC/DC converter, which means that the power flows from the PV to the load only and this is because the PV modules are only energy suppliers.

To obtain a stable voltage from the PV cells that is higher or lower than the output voltage, a high efficiency and minimum ripple DC-DC converter is required in the system [29]. The MPPT and the DC/DC converters designed for the storage devices are chosen to be a Buck-Boost converter so that it is possible to efficiently convert a DC voltage to lower or higher voltages, since the PV output voltage as well as the output voltage from the two storage elements are varying. In addition, the DC bus link voltage can be changed later according to the rated voltage of the motor.

4.3.1 Buck-Boost Converter for PV Panel (MPPT):

In this section, three different designs for the unidirectional Buck-Boost converter are proposed, where each time the design is improved in terms of the ripple current. Since X-series PV modules are selected due to their high efficiency, three modules will be connected in parallel to provide an output power of 1035 W at a voltage of 57.6 V. As can be seen from Table A-1, Table A-2 shown in Appendix A, and Table 4-2, each time the ripple current is assumed to be a certain percentage of the average inductor current, by improving from 30% to 10%. Regarding the prototype design in Table 4-3, it is decided to scale down the power to 200 W instead of 1035 W, to be able to implement the power converter and to work with the equipment provided in the lab.

Table 4-2 Third design of the Buck-Boost converter for PV.

Case 3			
Given		Required	
V_{in} (V)	57.6	D	0.455
P_{in} (kW)	1.035	R (Ω)	2.226
I_{in} (A)	17.969	I_L (A)	39.531
V_o (V)	48	L_{design} (μ H)	165.5
P_o (kW)	1.035	v_L (V)	57.6
I_o (A)	21.563	$\Delta i_{L,new}$ (A)	3.1625
Assumed		$I_{L,rms}$ (A)	39.626
f_s (kHz)	50	C_{design} (μ F)	408.381
T_s (μ s)	20	$V_r/V_{o_{new}}$ (%)	1
Δi_L (A)	3.953	V_C (V)	48
V_r/V_o (%)	2	V_d (V)	105.6
		V_s (V)	105.6

Table 4-3 Prototype design of the Buck-Boost converter for PV.

Prototype Design			
Given		Required	
V_{in} (V)	30	D	0.615
P_{in} (W)	200	R (Ω)	11.520
I_{in} (A)	6.667	I_L (A)	10.833
V_o (V)	48	L_{design} (μ H)	142.012
P_o (W)	200	v_L (V)	48
I_o (A)	4.167	$\Delta i_{L,new}$ (A)	2.6
Assumed		$I_{L,rms}$ (A)	11.065
f_s (kHz)	50	C_{design} (μ F)	213.675
T_s (μ s)	20	$V_r/V_{o_{new}}$ (%)	0.5
Δi_L (A)	3.250	V_C (V)	48
V_r/V_o (%)	1	V_d (V)	78
		V_s (V)	78

The modelling of the unidirectional Buck-Boost design is developed by Matlab/Simulink, the aim of this Simulink model is to design a Buck-Boost converter for the PV modules to step up 30 V input to 48 V output, which results in a duty cycle of $D=0.615$. Thus, a control signal of 0.615 duty cycle is generated and fed to the gate of the IGBT switch. The output voltage and its ripple and inductor current and voltage waveforms are presented in Figure 4-5. The capacitor at the load is added to remove the ripple and provide a DC output; however, there is still some ripple at the output side.

As shown in Figure 4-5, the output voltage across the load is approximately 48 V through the ON and OFF period of the switch, thus the results of the Buck-Boost converter are achieved successfully.

The inductor voltage and current waveforms are shown, such that when the switch is ON, the inductor voltage is equal to V_{in} , with increasing current of minimum and maximum values equal to the computed values. While when the switch is OFF, the voltage of the inductor is equal to $-V_o$, with decreasing current of minimum and maximum values. It can be noticed that the Buck-Boost converter is operating at the continuous conduction mode, since the minimum inductor current value is higher than 0 A.

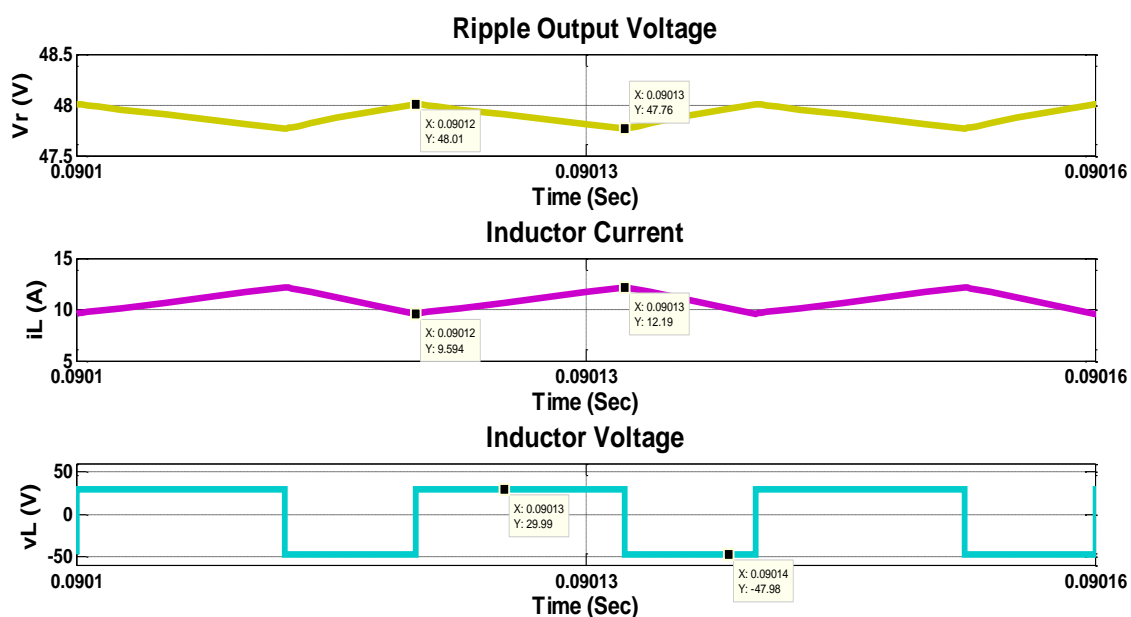


Figure 4-5 Ripple output voltage, inductor voltage and current waveforms for Buck-Boost converter.

4.3.2 Buck-Boost Converter for Battery

A typical lithium ion battery has a minimum power density of 100 Wh/kg, and rated power of 250 W/kg [33]. Thus, according to the race regulations, a Li-ion of 20 kg has a power density of 2 kWh and rated power of 5 kW. Since the rated voltage of battery packs is multiple of 12 V, it is assumed that the rated voltage of the Li-ion battery is 72 V, and so do the capacity of the battery is approximately 28 Ah. Table 4-4 shows the design values of the power converter, however, for the same reason mentioned earlier, the design is scaled down as shown in Table 4-5.

Table 4-4 Design of the Buck-Boost converter for Battery.

Design			
Given		Required	
V_{in} (V)	72	D	0.4
P_{in} (kW)	5	R (Ω)	0.461
I_{in} (A)	69.444	I_L (A)	173.611
V_o (V)	48	L_{design} (μ H)	41.472
P_o (kW)	5	v_L (V)	72
I_o (A)	104.167	$\Delta i_{L,new}$ (A)	13.889
Assumed		$I_{L,rms}$ (A)	174.027
f_s (kHz)	50	C_{design} (μ F)	17361
T_s (μ s)	20	$V_r/V_{o_{new}}$ (%)	1
Δi_L (A)	17.361	V_C (V)	48
V_r/V_o (%)	2	V_{s1} (V)	120
		V_{s2} (V)	120

Table 4-5 Prototype design of the Buck-Boost converter for Battery.

Prototype Design			
Given		Required	
V_{in} (V)	30	D	0.615
P_{in} (W)	100	R (Ω)	23.04
I_{in} (A)	3.333	I_L (A)	5.417
V_o (V)	48	L_{design} (μ H)	284.024
P_o (W)	100	v_L (V)	48
I_o (A)	2.083	$\Delta i_{L,new}$ (A)	1.3
Assumed		$I_{L,rms}$ (A)	5.532
f_s (kHz)	50	C_{design} (μ F)	53.419
T_s (μ s)	20	$V_r/V_{o_{new}}$ (%)	1
Δi_L (A)	1.625	V_C (V)	48
V_r/V_o (%)	2	V_{s1} (V)	78
		V_{s2} (V)	78

4.5.1 Buck-Boost Converter for Ultra-capacitors:

Since the ultra-capacitors are used as a second energy storage device, it was assumed that the rated power of the ultra-capacitors is 30% of the lithium ion battery. Table 4-6 and Table 4-7 show the actual and the prototype design respectively.

Table 4-6 Design of the Buck-Boost converter for Ultra-capacitors.

Design			
Given		Required	
V_{in} (V)	72	D	0.4
P_{in} (W)	1500	R (Ω)	1.536
I_{in} (A)	20.833	I_L (A)	52.083
V_o (V)	48	L_{design} (μ H)	46.08
P_o (W)	1500	v_L (V)	72
I_o (A)	31.25	$\Delta i_{L,new}$ (A)	12.5
Assumed		$I_{L,rms}$ (A)	53.196
f_s (kHz)	50	C_{design} (μ F)	520.833
T_s (μ s)	20	$V_r/V_{o_{new}}$ (%)	1
Δi_L (A)	15.625	V_C (V)	48
V_r/V_o (%)	2	V_{s1} (V)	120
		V_{s2} (V)	120

Table 4-7 Prototype design of the Buck-Boost converter for Ultra-capacitors.

Prototype Design			
Given		Required	
V_{in} (V)	30	D	0.615
P_{in} (W)	100	R (Ω)	23.04
I_{in} (A)	3.333	I_L (A)	5.417
V_o (V)	48	L_{design} (μ H)	284.024
P_o (W)	100	v_L (V)	48
I_o (A)	2.083	$\Delta i_{L,new}$ (A)	1.3
Assumed		$I_{L,rms}$ (A)	5.532
f_s (kHz)	50	C_{design} (μ F)	53.419
T_s (μ s)	20	$V_r/V_{o_{new}}$ (%)	1
Δi_L (A)	1.625	V_C (V)	48
V_r/V_o (%)	2	V_{s1} (V)	78
		V_{s2} (V)	78

4.4 Electric Motor

The first component that should be selected is the motor since the output specifications of the battery pack and the PV array are ruled by the necessities of the motor [34]. This motor should own suitable torque, extremely high efficiency, low mass, and the correct amount of power and speed [34]. It is decided to choose a BLDC motor due to its high power to weight ratio, high efficiency and ease of control [34]. There are two main types of BLDC motors axial flux and radial flux, the difference between them is the flow of flux. In radial flux permanent magnet (RFPM), the flux flows radially around the stator, however, in axial flux permanent magnet (AFPM), the flux flows axially along the axis of the stator. To further illustrate, in RFPM, permanent magnets (PMs) and armature windings are radially arranged as shown in Figure 4-6, where the PMs are parallel to the shaft of the machine [35]. In AFPM, permanent magnets (PMs) and armature windings are axially arranged as shown in Figure 4-7, where the PMs are perpendicular to the shaft; consequently the flux lines are parallel to it [35].

Generally, solar cars use axial flux motors, unlike traditional motors that depend on the radial flux for propulsion. The alignment of magnetic fields with respect to the central axis of revolution affects the flux direction.

In axial flux motors, the air gap can be adjusted to affect the motor torque-speed characteristics. The term air gap refers to the distance between the PMs located on the rotor and the electromagnetic coils located on the stator. Regardless the speed, some teams adjust the air gap on the fly to operate at maximum efficiency [13]. This axial flux BLDC typically draws approximately 2 kW [3].

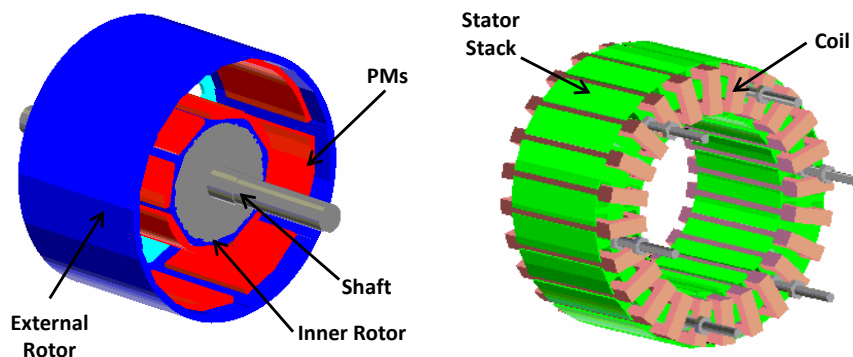


Figure 4-6 Radial flux permanent magnet machine [36].

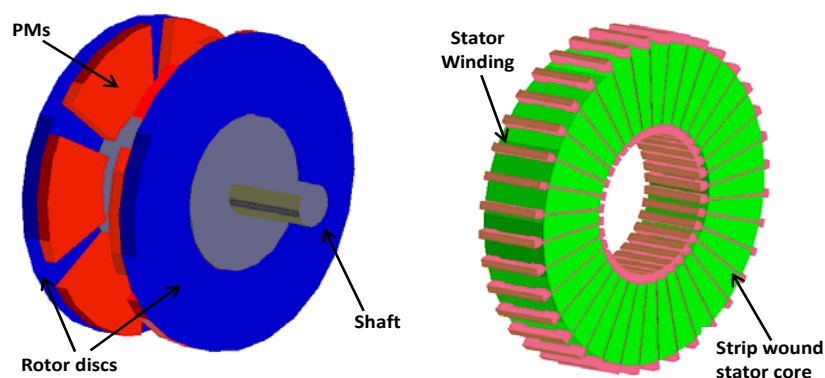


Figure 4-7 Axial flux permanent magnet machine [36].

There are two different drive systems [37], the first one is when the motor is installed on the shaft between the two wheels, where wheels receive power from the motor via the drive shaft as shown in Figure 4-8 [37], this will run the wheels at the same speed, thus differential gear is used to allow the drive wheels to turn at different speeds when both receives power from the motor. To further explain, turning right means that the left wheel travels more distance at a higher speed when compared to the right wheel [38]. The differential gear mechanism is important in such scenario; however differential gear has low efficiency.



Figure 4-8 Single motor driving the wheels through a gearbox drive shaft.

The other one is the in-wheel motor (IWM), where motors are installed in the wheels of the car as shown in Figure 4-9 [37]. In-wheel hub motors are electric motors that are installed close to each of the drive wheels, and move the wheels through small drive shafts. One of the merits of in-wheel motors is the high efficiency, since the power flows directly from the motor to the wheel, thus the

distance is reduced and the efficiency increases making it possible to control the wheels precisely. In addition, in-wheel motors produce high amount of torque, and few of it is lost in the transfer, since that force is directly transmitted to the wheel. However, installing two motors instead of one is more expensive, in addition in-wheel motors are exposed to more vibrations and dirt. It is decided to use two in-wheel motors installed on the rear wheels (the front wheels are left for the steering system) where each one draws 1kW to propel the car due to the four wheel design.



Figure 4-9 Two in-wheel hub motors driving the wheels through very small drive shafts.

4.5 Steady state analysis of energy management system (EMS)

During solar car racing, the car is driven with speed variations in response to the road conditions and the solar power. Consequently, this leads the teams to design their cars so that it should be driven at the maximum efficiency not only at a constant speed during long distances, but also at sharp corners where the car should be able to accelerate and brake, especially that frequent acceleration and braking actions lead to large and rapid drops and rises in the motor current.

Figure 4-10 describes the flow of energy into the system, and the flow of energy from and to the energy storage devices [39]. The flow of power from the PV array is varying depending on the environmental conditions; this power value expresses the quantity of solar energy converted into electrical energy [39]. The energy drawn from the PV is allocated for the drive system and the battery [39]. The current flowing into or from the battery is labelled as I_B , it is represented as a positive quantity if the battery is feeding the load. In other words, when the car accelerates, power flows to the load and the battery discharges. However, in deceleration situations, current flows back from the motor to the battery and the battery charges. The current flowing into or from the ultra-capacitors is labelled as I_C , as shown in Figure 4-10, it can flow in both directions depending on the load requirements, it could be negative in regenerative braking conditions, where it is highly required to charge the ultra-capacitors to get use of the energy. The load current can be expressed as [40]:

$$K_{Load}I_{Load} = K_{PV}I_{PV} + K_B I_B + K_C I_C$$

Where;

K_{Load} : Sign of the load current (1, -1)

K_{PV} : Sign of the PV current (0, 1)

K_B : Sign of the battery current (0, 1, -1)

K_C : Sign of the ultra-capacitors current (0, 1, -1)

I_{Load} : Load current in amperes.

I_{PV} : PV array contribution in the DC bus in amperes.

I_B : Battery contribution in the DC bus in amperes.

I_C : Ultra-capacitors contribution in the DC bus in amperes.

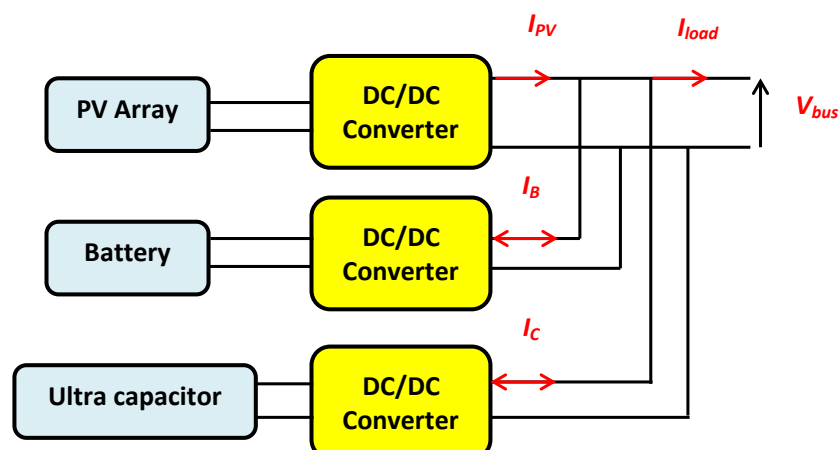


Figure 4-10 Energy management.

There are four different situations where the load current varies; the first situation is high speed where the load current increases when the speed increases [40]. The second situation is when the car is moving at a constant speed, the load current is constant. Another situation is deceleration where the load is characterized by its negative current. The last situation is the null speed, where the load current is zero [40].

The load current is shared between the three sources: PV array, battery, and ultra-capacitors according to the dynamics of the sources [40]. The PV contribution in the DC bus is presented in two states:

- 1) During the day ($K_{PV} = 1$).
- 2) At night ($K_{PV} = 0$).

However, the battery and the ultra-capacitors are represented in three states [40]:

- 1) Positive contribution in traction operation ($K_B = 1, K_C = 1$).
- 2) Negative contribution in deceleration and braking operations ($K_B = -1, K_C = -1$).
- 3) Null contribution at null speed or when the PV is delivering the required power ($K_B = 0, K_C = 0$).

The energy is managed based on the current situations during the race, where many circumstances should be taken into considerations such as:

- a. High speed conditions: at high speed, PV modules will not be able to work without the need of another storage device, since increasing the speed will lead to more power consumption by the motor. Thus, more power should be generated to drive the car by the battery and/or the ultra-capacitors as shown in Table 4-2 in case 1.
- b. Deceleration conditions: in braking conditions, it is a must to draw the power back to the ultra-capacitors and if the ultra-capacitors were fully charged, then the battery could be used to store the rest of the energy. In other words, if the load current is negative, then it is recommended to store the energy in the ultra-capacitors, rather than the battery, and to store the PV energy in the battery as shown in case 3 in Table 4-2.

- c. Time: is an important factor that should be taken into consideration, if it is night, then the power drawn from the PV is zero, and here where the energy storage devices should work efficiently to deliver the required power to the load as shown in case 2 and case 4 in Table 4-2.
- d. Route: the road conditions also play an important role in how the energy is managed. If the driver is away 500 m from a turn, then the ultra-capacitors should be discharged so that when decelerating the energy is stored in the ultra-capacitors.
- e. Level of charging and discharging: the energy storage devices should be charged and discharged at certain levels, and if the specified levels are exceeded then no action should be taken.

Table 4-8 Different conditions of the power flow according to the load conditions.

Cases	K_{Load}	K_{PV}	K_B	K_C
Case 1	+1	+1	+1	+1
Case 2	+1	0	+1	+1
Case 3	-1	+1	-1	-1
Case 4	-1	0	-1	-1

When the vehicle is cruising, the energy demand is not high, thus the voltage drop of the battery is neglected. However, at climbing slope or accelerating, as mentioned earlier the motor would cause a large current impulse, which will lead to a high voltage drop in the battery affecting the power quality of the DC bus [20]. In addition, the large current discharge level will decrease the battery lifetime. Thus, the employment of ultra-capacitors with its bidirectional power converter in parallel with the battery will save energy and avoid such a problem [20]. To further explain, when there is a rapid rise in the current, the bidirectional power converter will be controlled as a current source to supply the extra load current, preventing the battery current from exceeding specific values, and so do voltage drop is avoided and longer battery lifetime is acquired [20].

The following EMS flowchart shows the importance of monitoring the voltage of the battery and the capacity of the ultra-capacitors, where certain actions should be taken when the measured parameters are not within the specified limits, otherwise different EMS cases can be applied.

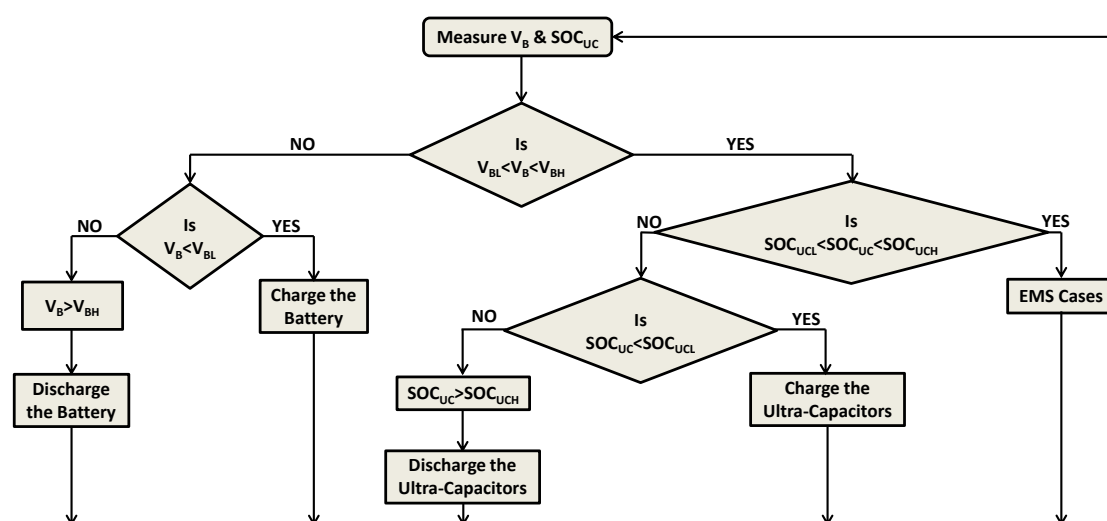


Figure 4-11 EMS flowchart.

4.6 Topologies

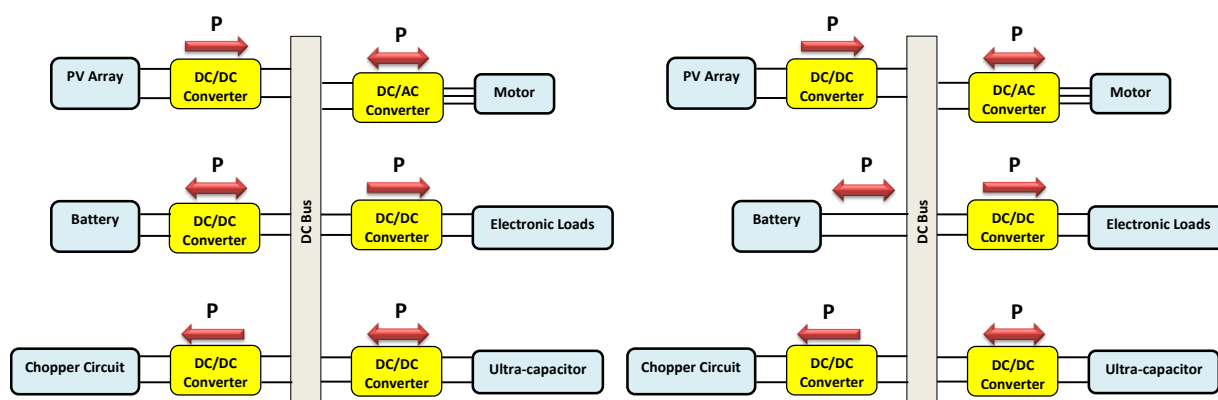


Figure 4-12 First topology.

Figure 4-13 Second topology.

Different topologies are studied, and from these topologies only two are chosen as desired scenarios for practical implementation. In the first topology shown in Figure 4-12, the battery is connected to the DC bus through a bidirectional DC/DC converter, however, in the second topology shown in Figure 4-13, the battery is directly connected to the DC bus. Connecting the battery without a power converter will keep the voltage of the DC bus floating, this will cancel the need of extra current and voltage transducers and each source will control its energy, since in this topology, it is not obligatory to fix the output current at other sources to a certain value as in the first topology. Hence, the second topology shown in Figure 4-13 which is the open loop control scheme is selected to be implemented; since the first topology shown in Figure 4-12 which is the closed loop control scheme is more complex from the practical point of view, in addition, one converter is eliminated in the second topology. As can be noticed in Figure 4-12 and Figure 4-13, a chopper circuit is added to absorb the extra energy if none of the sources can handle this extra energy. In other words, the addition of this chopper circuit is because of the surplus power situations, where the extra power should be dissipated through a converter with a certain duty cycle, however, it is a rare case and it is just added for the purpose of protection and safety complying with the WSC standards.

According to the regulations of the WSC competition, there is a degree of freedom for selecting the DC bus voltage. Since the power drawn by the BLDC motor is relatively high, it is highly recommended to increase the DC bus voltage to decrease the current; consequently the size of the components and the wires will reduce. Thus, it is suggested to select the bus voltage to be 48 V as discussed in the previous sections.

From the practical point of view, the electric loads such as the brakes, the conditioning system, and the radiator fans can be considered as a constant load, as well as the chopper circuit and the motor. Hence, practically, the chopper circuit, the electrical loads, and the motor are considered as a load.

Chapter 5 : PRACTICAL IMPLEMENTATION

This chapter presents the practical implementation of both the MPPT and the different cases of the open loop energy management system of a solar car. In addition, this chapter presents the designed software program using Matlab/Simulink and the project's test rig, in addition to overall system hardware connection. The power converters are designed such that they operate in continuous conduction mode to have lower losses and consequently, higher efficiency when compared to the discontinuous conduction mode; this is done to fulfil the constraints mentioned in section 2.5, since vehicle efficiency is a main factor for success. Besides, practical results are discussed and compared to the expected results.

5.1 Controller

DSPs are capable of controlling algorithms with high flexibility, reducing components, and introducing testing procedures. DSPs achieve a very high sampling rate with high performance. The eZdsp F28335 is a stand-alone card that evaluates the TMS320F28335 Digital Signal Controller (DSC) operating at 150 MHz with an on chip 32-bit floating point, and an on chip 12-bit Analog to Digital (A/D) converter with 16 input channels [41]. The board has multiple expansion connections to interface to all F28335 I/O signals [41]. In addition, built in CAN and RS-232 connectors are available [41]. It also has a built in USB to embedded JTAG emulator for software debug and flash programming [41]. The eZdsp F28335 board is supplied by a +5 V provided AC adapter, however, it supports +3.3 V Input/Output levels which are not +5 V tolerant [41]. Regarding the Software features, a Code Composer Studio Integrated Development Environment for C2000 including C compiler, assembler, linker, and debugger is provided to simplify code development and shorten debugging time. The DSP MCU is connected to the Matlab/Simulink software in the computer through the Code Composer Studio, which provides interface by debugging. In this project, the DSP is used to generate the PWM signal. In addition, the ADC pins are used to convert the analog measurements by the transducers into digital.

5.2 Gate Drive Circuit

The gate drive circuit is a power amplifier that accepts low-power input signal (PWM signal) from a controller (eZdspF28335) and produces a high-current drive input to the gate of a high-power transistor such as an Insulated-Gate Bipolar Transistor (IGBT). The gate drive circuit provides isolation between the control signal and the IGBT gate by means of two transformers. One transformer is for transmitting power from the low-side circuit and the other for transmitting the gate-drive signal. Looking at the top view of the gate drive board shown in Figure 5-1, there are two bottom connector pins on the left side that accepts the signal and its ground generated by the micro-controller. The gate drive board is powered by +5 Vdc/GND via the two top pins. The connector on the right side provides the signal with its reference that drives the IGBT via its gate and emitter connections.

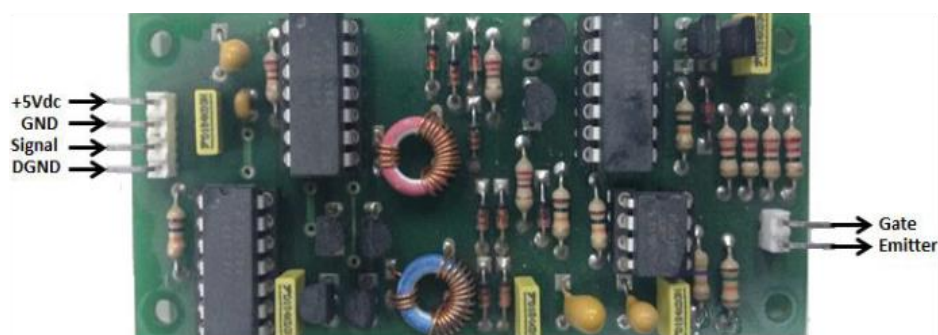


Figure 5-1 Gate drive board.

5.3 Voltage & Current Transducers

The voltage and current transducers are used to sense the PV voltage and current respectively, and scale them down to a certain level to be inserted to the DSP since the DSP cannot accept an input that is more than +3.3 V. This can be done by adjusting the gain of both transducers; however, the offset of both transducers must be adjusted to zero. Both voltage and current transducers use Hall Effect sensor; which is an analog transducer that varies its output voltage in response to a magnetic field.

For voltage measurements, LEM LV 25-P is used in which a current proportional to the measured voltage will pass through a resistor which is selected by the user according to the primary nominal voltage (maximum of 500 V), this resistor is installed in series with the primary circuit of the transducer, in addition a measuring resistance is added and selected according to the datasheet.

For current measurements, LEM LA 55-P is used in which the current sensor in the current transducer detects and converts the current to a scaled output voltage that is proportional to the nominal primary current (maximum of 50 A) passing through the path. A measuring resistance is added and selected according to the datasheet. The reason for selecting LEM transducers is due to their high accuracy and their good linearity.

The calibrations of both transducers are shown in Figure B-4 in Appendix B, where the gain is set to a certain value such that no more than a 3 V signal enters the ADC pins of the DSP.

5.4 Software

In order to test the MPPT, it is firstly preferred to plot the P-V curve of the PV in order to identify the MPP on the curve and to verify that the MPPT is tracking this point. This is done by generating a PWM signal with a variable duty cycle and 50 kHz switching frequency from the digital signal processor (DSP) via Matlab/Simulink, it is decided to use a switching frequency of 50 kHz since practically the gate drive circuit could burn if the switching frequency is higher than 50 kHz. Three different blocks are used as shown in Figure 5-2 in order to generate the P-V curve of the PV; Sine Wave, Fcn and ePWM blocks. Then, in order to show the MPP, eight different blocks are used as shown in Figure 5-2; ADC, two Zero-Order Holds, two Gains, three Fcns, Embedded Matlab Function, Saturation and ePWM blocks. Pulse Generator and Switch blocks are used to plot both the P-V curve

and the MPP with a difference of 10 seconds since the P-V curve is changing from time to time due to the weather conditions and to ensure that the MPPT is tracking the MPP regardless the conditions.

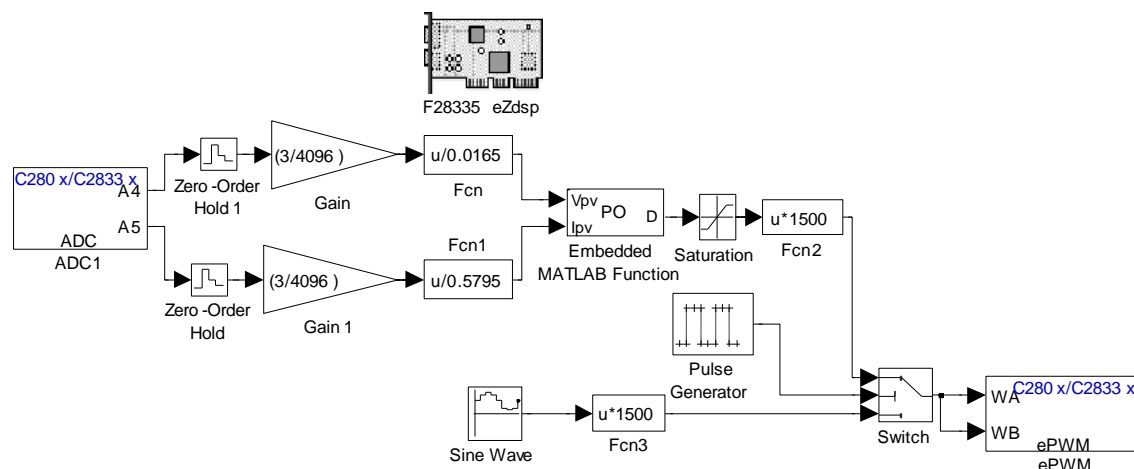


Figure 5-2 Matlab/Simulink simulation for generating the PWM signal for tracking the PV MPP.

The Sine Wave block is used to generate the PWM signal with a variable duty cycle from 0 to 0.9; hence, the Sine Wave amplitude is set to 0.45 and the bias is set to 0.45. The Fcn block is used to generate the 50 kHz switching frequency of the PWM signal seeing that the MCU frequency of the available DSP is 150 MHz, while the required switching frequency is 50 kHz, thus the time period is $\frac{150 \text{ MHz}}{50 \text{ kHz}} = 3000$ counts, however, this 3000 counts are set to 1500 counts. The ePWM block has 16 ePWM modules configurable to service event managers A and B. The ePWM block parameters have been modified where ePWM1 module is selected, the Time period value is set to 1500 counts, and the Counting mode is selected to be up/down mode due to its symmetry.

The TMS320F28X ADC module is a 12-bit analog-to-digital converter (ADC). The ADC module has 16 channels, configurable as two independent 8-channel modules to service event managers A and B. The ADC block parameters have been modified where the Data type has changed to double since two wires have been used; one for the signal and the other is for its reference, ADCINA4 and ADCINA5 are also selected to be used from the 16 channels to convert two conversions; one for the voltage transducer and one for the current transducer, as shown in Figure 5-2. The two Zero-Order Hold blocks are used to slow down the sampling process for the two ADC conversions. The two Gain blocks are used to convert the digital values obtained from the ADC to analog values again. The gain value is set to $\frac{3}{4096}$ since the ADC on the DSP converts the 3 V to 4096 counts, and hence the gain value is the reciprocal of $\frac{x \text{ V} * 4096}{3 \text{ V}}$. The two Fcn blocks are used as a scaling factor for the voltage and current transducers. Their expressions are set based on the equations obtained from the voltage and current transducers calibration process as shown in Figure B-4 in Appendix B. Embedded Matlab Function block is used to write the code representing the P&O algorithm as shown in Figure B-3 in Appendix B. The Saturation block is used to limit the duty cycle with a lower limit of 0.1 and an upper limit of 0.8.

5.5 Hardware

This section presents the project’s test rig, the overall system hardware connection, and clarifies the system parameters, including the PV panel, battery, ultra-capacitors, and the load. Figure 5-3 shows the experimental setup and Figure 5-4 shows the overall hardware connection of the designed system.

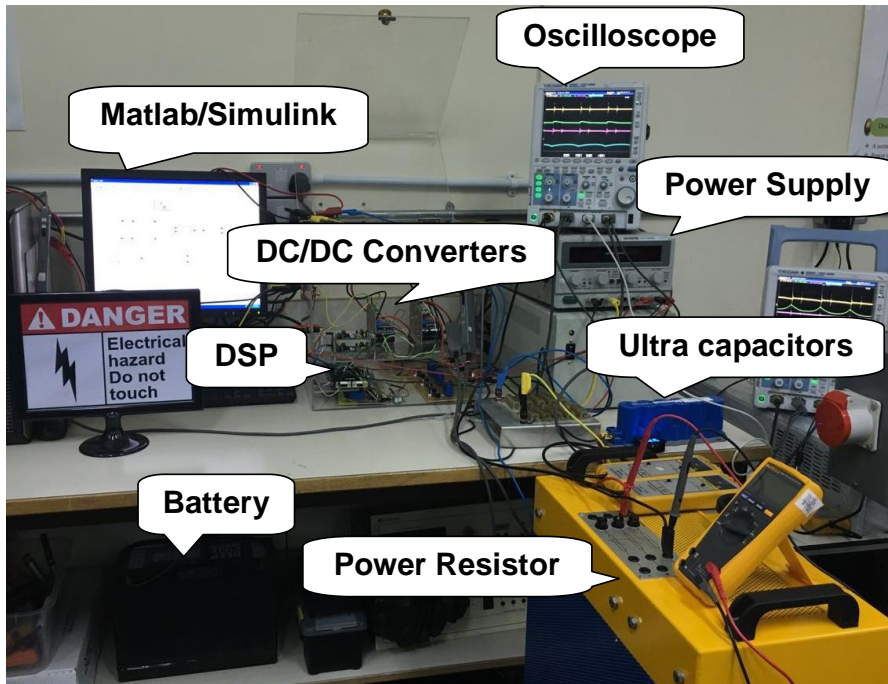


Figure 5-3 Test rig.

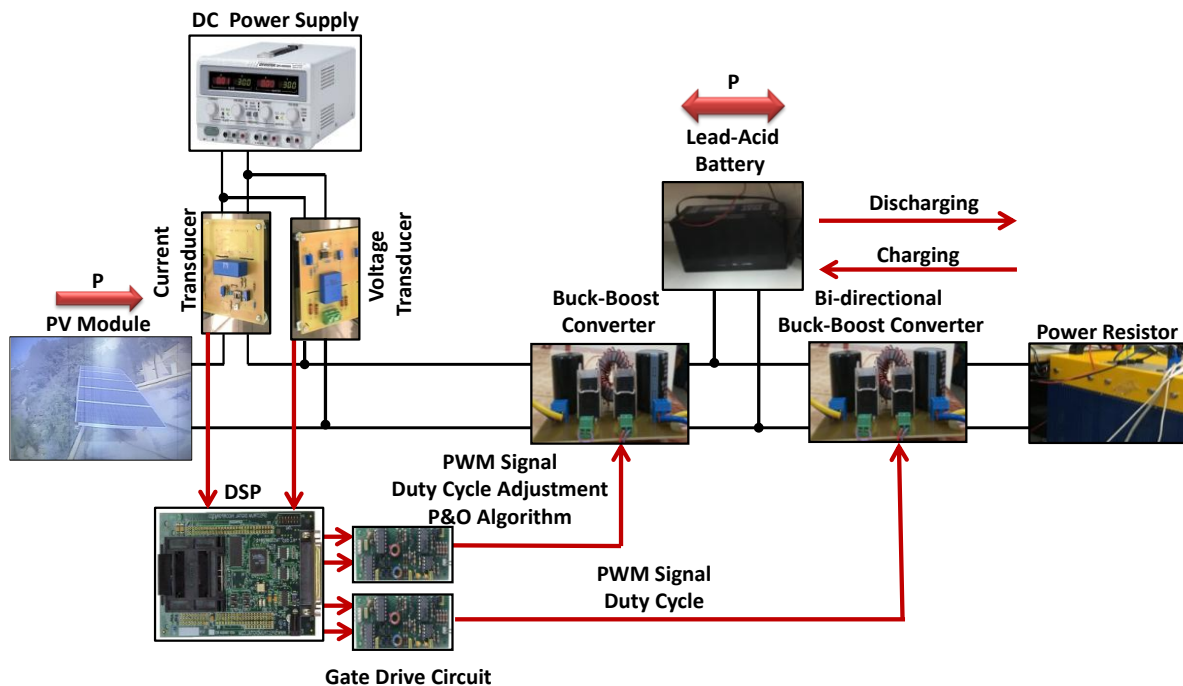


Figure 5-4 Overall system hardware connections.

Table 5-1 System parameters

System Parameters		
PV Panel	Open Circuit Voltage V_{oc}	40 V
	Short Circuit Current I_{sc}	4 A
	Maximum Power P_{mpp}	120 W
Battery	Battery Type	Lead-Acid
	Nominal Voltage V_B	12 V
	Rated Capacity	100 Ah
Ultra-capacitors	Voltage V_{uc}	16.2 V
	Capacitance	58 F
Resistive Load	Power	3.3 kW

5.6 Results & Discussion

Since the main aim of this project is to manage the flow of energy up to the DC bus, thus, to test the system a static load is chosen. This section presents the experimental results of the designed Buck-Boost converters, MPPT using P&O technique, different energy management cases at different conditions. In addition, performance assessment of the implemented system is shown to see the behaviour of the voltage, current, and power of all sources by increasing the resistive load. Moreover, the project cost as well as the design limitations of this project is clarified.

5.6.1 Buck-Boost Converter:

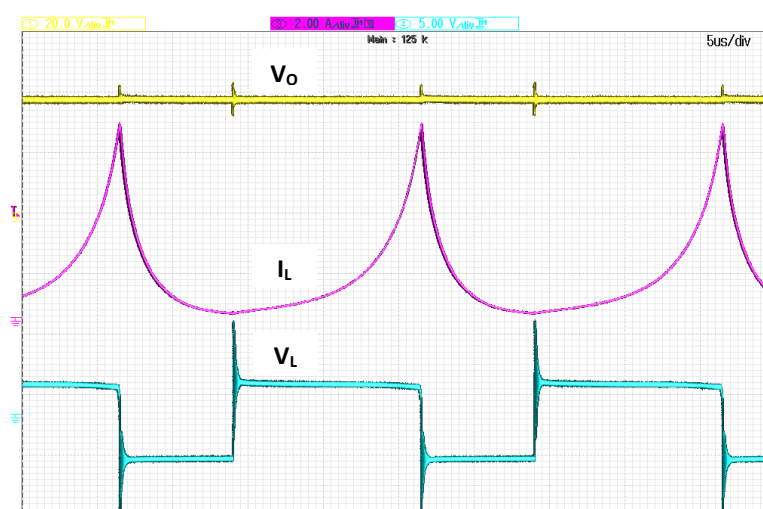


Figure 5-5 Output voltage and its ripple, Inductor current and voltage waveforms.

The oscilloscope channels are connected to the output connectors to observe the voltage waveforms, and as shown in Figure 5-5, the output voltage is (44 V). It is noticeable that the obtained values are not exactly equal to the designed values, the reason behind that is due to the non-ideality of the components. In other words, this is due to the effect of the parasitic elements in the switch, the inductor, and the capacitor, which lowers the converter efficiency. It is observed that the obtained ripple voltage is less than the expected value, since the practical capacitor value is selected to be greater than the deigned capacitor value.

The inductor voltage and current waveforms are shown in Figure 5-5. Such that when the switch is ON, the inductor voltage is equal to V_{in} , and the inductor current increases, however, the maximum and minimum inductor voltage are scaled down by a factor of 10, since the differential probe is used.

While when the switch is OFF, the voltage of the inductor is equal to $-V_o$, and the current decreases. It can be noticed that the practical inductor current waveform shown in Figure 5-5 is not exactly a ramp as expected. This is due to the practical inductor core, which operates near its saturation region. Mostly, when designing a converter, the inductance is designed to be far from the saturation region, because otherwise it will cause nonlinear behaviour for the inductor current. When an inductor enters or it is near the saturation, the up slope of the inductor current is increased, which means that the inductance is decreased. However, the inductor continues to store energy even though it is operating in the saturation region, as it will recover during the down slope.

5.6.2 Maximum Power Point Tracker MPPT:

This section shows the obtained MPPT results using P&O algorithm at different perturbation sizes, to see and observe the behaviour of the system using different step sizes.



Figure 5-6 PV array power, voltage, and current waveforms at the MPP with 10 W/div, 10 V/div, and 1 A/div respectively, and with a perturb size of 10^{-7} .

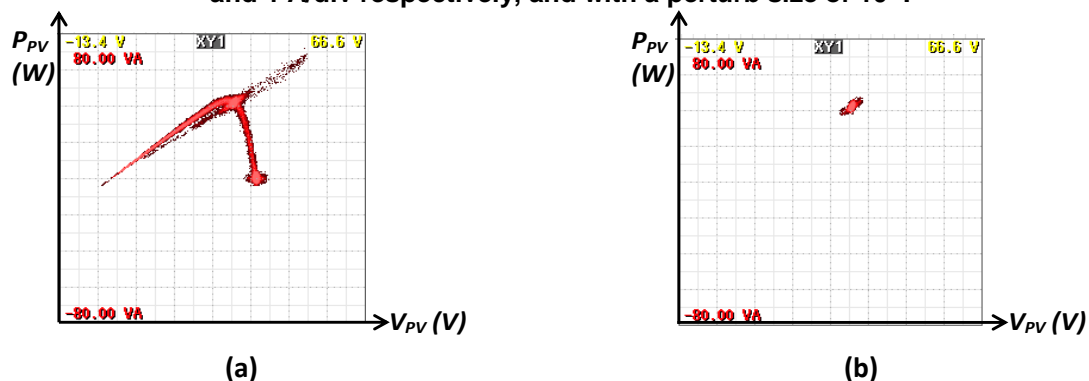


Figure 5-7 MPPT results at perturb size of 10^{-7} : (a) P-V curve at variable duty cycle; (b) Maximum power point.

A PV array with an open circuit voltage V_{OC} of 40 V and a short circuit current I_{SC} of 4 A is used with the MPPT experimental setup. Figure 5-6 and Figure 5-7 show the obtained results from the implemented MPPT at a perturb size of 10^{-7} . It is noticeable from Figure 5-6 that the PV array is operating at a voltage (V_{mpp}) corresponding to the MPP (32 V) which is approximately 80 % of the open circuit voltage. In addition, it is observable that the PV is not operating at the I_{mpp} , and this is due to the cloudy conditions, since as the insolation level decreases the short circuit current decreases. It is clearly seen from Figure 5-7 (b) that the MPPT is exactly operating at the MPP and this could be

verified from the P-V curve shown in Figure 5-7 (a) that has the same scale as the P-V graph shown in Figure 5-7 (b).

Figure 5-8 and Figure 5-9 show the PV power, voltage, and current waveforms with a perturbation size of 0.01 and 10^{-7} respectively. Obviously, it can be said that at a high perturbation size, the system reaches the MPP faster, however, the oscillations increases. While, at low perturbation size, the number of oscillations decreases, however, this way slows down the algorithm response. In other words, fast dynamic response is achieved by large perturbation size; however, reduced oscillations are achieved by small perturbation size. Hence, it is concluded that there is a trade-off between faster time response and steady state oscillations.

During cloudy days, the solar insolation levels vary many times, and this reduces the efficiency of the MPPT, thus it is necessary to achieve a good dynamic response to avoid losing a great quantity of energy. The efficiency of the P&O technique depends on the perturbation size, and it is difficult to obtain the optimal perturbation size, thus it is suggested to work with a variable perturbation size to obtain a faster dynamic response with small oscillations. This is called adaptive P&O technique that operates with variable perturbation size depending on the current operating conditions. To further illustrate, large perturbation steps are chosen when the operating point is far from the MPP and small perturbation steps are chosen when the operating point is close to the MPP.



Figure 5-8 PV array power, voltage, and current waveforms at the MPP with 4 W/div, 20 V/div, and 200 mA/div respectively, and with a perturbation size of 0.01.



Figure 5-9 PV array power, voltage, and current waveforms at the MPP with 4 W/div, 20 V/div, and 200 mA/div respectively, and with a perturbation size of 10^{-7} .

5.6.3 Energy Management System:

In this section, different cases are considered according to the requirements of the load.

A. Case 1:

The first case that is considered is shown in Figure 5-10, where the following are the operating conditions:

- 1) The PV is operating at the MPP and the power is equal to 53 W.
- 2) The battery has a state of charge which is: $SoC_L \leq SoC \leq SoC_H$ (20% $SoC \leq SoC \leq 80\%$ SoC), and the voltage is within the specified limits, where: $V_{BL} \leq V_B \leq V_{BH}$ (10 V $\leq V_B \leq 14$ V).
- 3) The ultra-capacitors have not connected to the system yet.

In this case the results are taken at 1:30 pm, where the PV is operating at the MPP and the duty cycle of the converter connected to the PV panel is 0.27. Although the maximum power that can be drawn from the used PV panel is 120 W, however, the power at that time was 53 W, since it was a cloudy day and the short circuit current was low. The Buck-Boost converter connected between the battery and the resistive load is set to a duty cycle equals to 0.5, so that the load voltage is equal to the battery voltage. The PV power is shared between the load and the battery where the resistive load is set to 10 Ω . The results are shown in the following single line diagram where the efficiency of each converter and the power losses are stated, as well as the operating voltage, current, and power for each source.

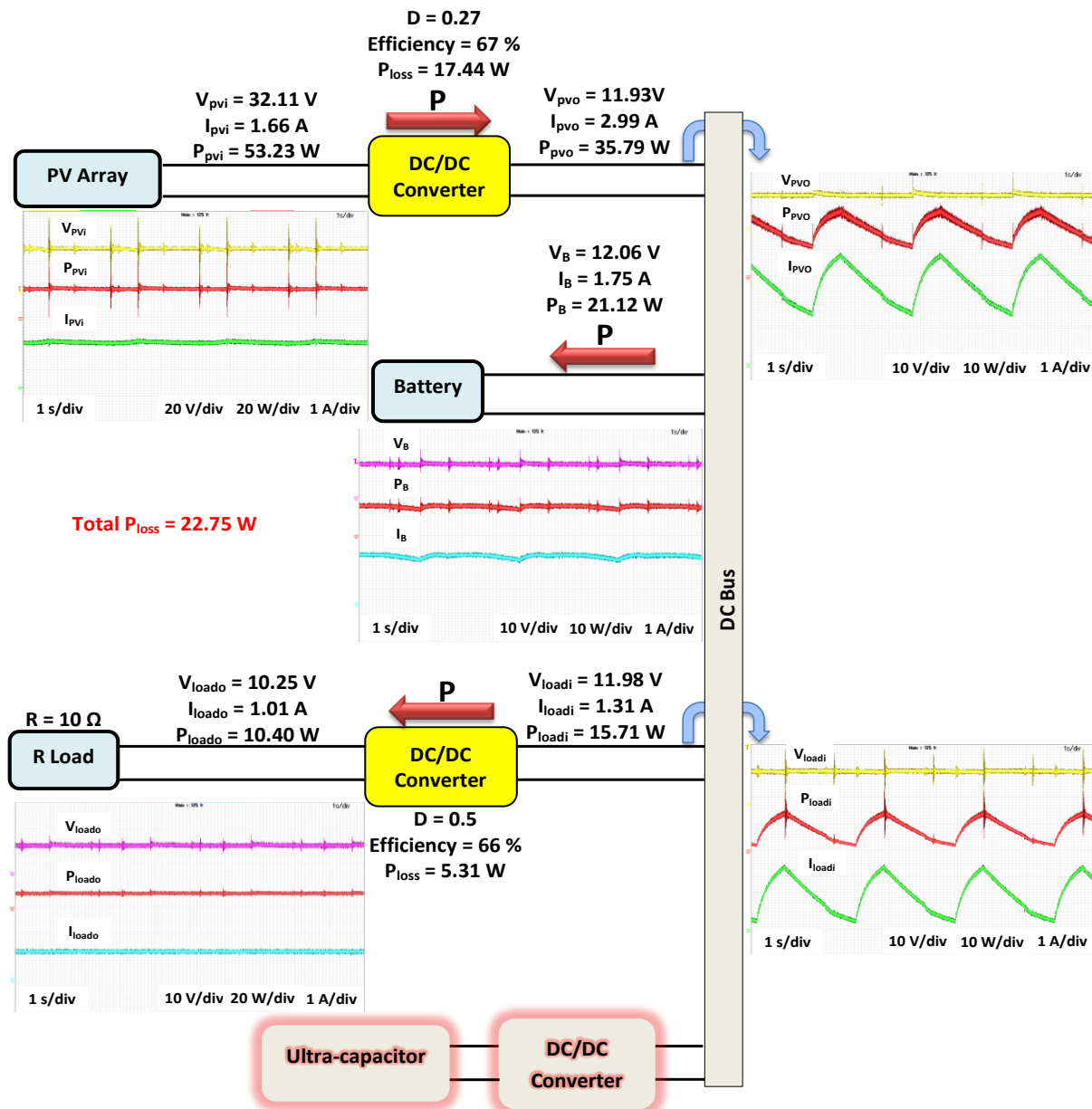


Figure 5-10 Charging case single line diagram.

It is observed from Figure 5-10, that the output voltage of the DC/DC converter connected between the PV and the battery is not the same which is not expected, and this is due to measurement errors. This can be avoided by taking the measurements more than one time using different probes. It can be noticed from Figure 5-10 that the power loss is high, which results in low efficiency for the two converters. This is due to the fact that the converters are designed for high power ratings, which are in the range of kilowatts, however, the input power of the converters is in watts. In addition, in order to address high power, high current will be drawn from the battery since the DC bus voltage is 12 V and the system is designed such that the DC bus voltage is 48 V. Therefore, high current will cause high power losses and hence, low efficiency. The IGBTs used in these converters can sustain up to 1000 V and 60 A. In other words, the designed converters are addressing high power; however, they are being used for low power ratings. In addition, the IGBT tends to be the main component responsible

for the high power loss, which results in low efficiency. To further illustrate, IGBT is a semiconductor device that works in two states and produces losses in those two states which are: switching losses and conduction losses. An IGBT module consists of an IGBT and a built-in fast recovery diode, and each one of these leads to different power loss. A loss hierarchy of an IGBT module is shown in the following figure.

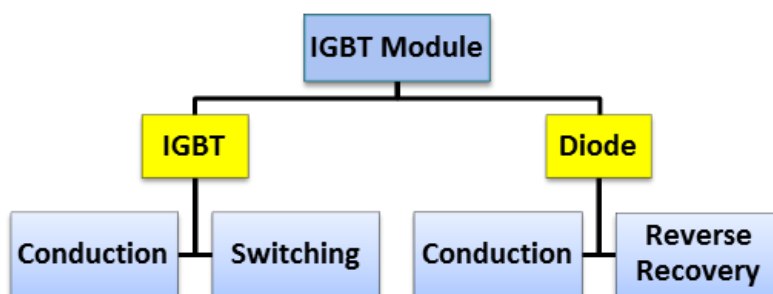


Figure 5-11 IGBT Module losses.

The switching losses are associated with the transition of the switch from its on state to its off state. Switching losses mainly depend on the switching frequency, load current, and the DC link voltage. Since the converters are designed to operate at 50 kHz switching frequency, thus it is expected that the losses will be high since the switching frequency is directly proportional to the losses. In other words, as the switching frequency increases, the states of the switch change in a faster manner, and hence the losses increase. To avoid this, it is preferable to work at a lower switching frequency, or to change the IGBTs to MOSFETs since they have higher switching capabilities, and hence lower power losses, which will lead to higher efficiency.

Lowering the switching frequency will lower the losses in the IGBTs as well as the inductor core, however, the value of the capacitors and the inductor must increase when decreasing the switching frequency to maintain an acceptable amount of output voltage ripple and inductor current ripple, which may not be acceptable in some applications. Hence, there is a trade-off between the switching frequency and the component's size.

Another factor that results in low efficiency is the conduction losses in the IGBT and the diode. Conduction losses are the losses that occur when the IGBT or the fast recovery diode is ON. Conduction losses mainly depend on the duty cycle and the load current. The conduction losses and the duty cycle have a direct relationship. Moreover, when the built-in diode turns off, it generates losses called the recovery losses. The power lost in the diode is due to the forward voltage drop which is approximately 0.7 V. A Schottky diode can be used since it has a lower voltage drop and short reverse recovery time; however, it is not used for high voltage applications.

It is worth mentioning that at low switching frequency, the conduction losses will dominate. On the other hand, for low duty cycle (less than 0.5); switching losses tend to dominate especially for high switching frequency. Thus, it can be said that the power loss in the first converter, which is the one connected between the PV and the battery has mostly resulted from the switching losses.

All of the mentioned losses are resulted only from the IGBT module, however, there are also losses that are resulting from the other parasitic elements, especially the inductor which introduces two types

of losses: core losses and winding losses, where the core losses depends on the magnetic characteristics of the core and the winding losses depends on the DC resistance of the coil that makes the inductor turns. Using a larger diameter wire will decrease the winding losses, and as mentioned earlier, decreasing the switching frequency will decrease the core losses; however, this will increase the cost but will achieve better efficiency.

It is noticed from Figure 5-10 that the efficiency of the two converters is close; the reason behind this is that there is a compromise between the input power and the duty cycle. To further illustrate, the first converter which is connected between the PV array and the battery operates at high power and low duty cycle, however, the second converter that is connected between the battery and the resistive load operates at a lower power but with a higher duty cycle.

It can be noticed from Figure 5-8 that the results are verified by applying Kirchhoff's Current Law, such that the input current at each node is equal to the output current from this node.

B. Case 2:

The second case that is considered is shown in Figure 5-12, where the following are the operating conditions:

- 1) The PV power is equal to 61 W.
- 2) The battery has a state of charge which is: $SoC_L \leq SoC \leq SoC_H$ (20% $SoC \leq SoC \leq 80\%$ SoC), and the voltage of the battery is within the specified limits, where: $V_{BL} \leq V_B \leq V_{BH}$ (10 V $\leq V_B \leq 14$ V).
- 3) The ultra-capacitors have not connected to the system yet.

In this case the results are taken at 12:30 pm, where the PV is operating at the MPP and the duty cycle of the converter connected between the PV panel and the battery is 0.27. The Buck-Boost converter connected between the battery and the resistive load is set to a duty cycle equals to 0.67, so that the output voltage of this converter is double the input voltage. In this case, the duty cycle is changed from 0.5 to 0.67 to avoid high current, especially that the DC bus voltage is equal to 12 V. According to the operating conditions mentioned earlier, the PV panel and the battery will supply the resistive load. This case is taken assuming that the load needs high power, and hence the needed power will be drawn from both the PV and the battery. The results are shown in the following single line diagram where the efficiency of each converter and the power losses are stated, as well as the operating voltage, current, and power for each source.

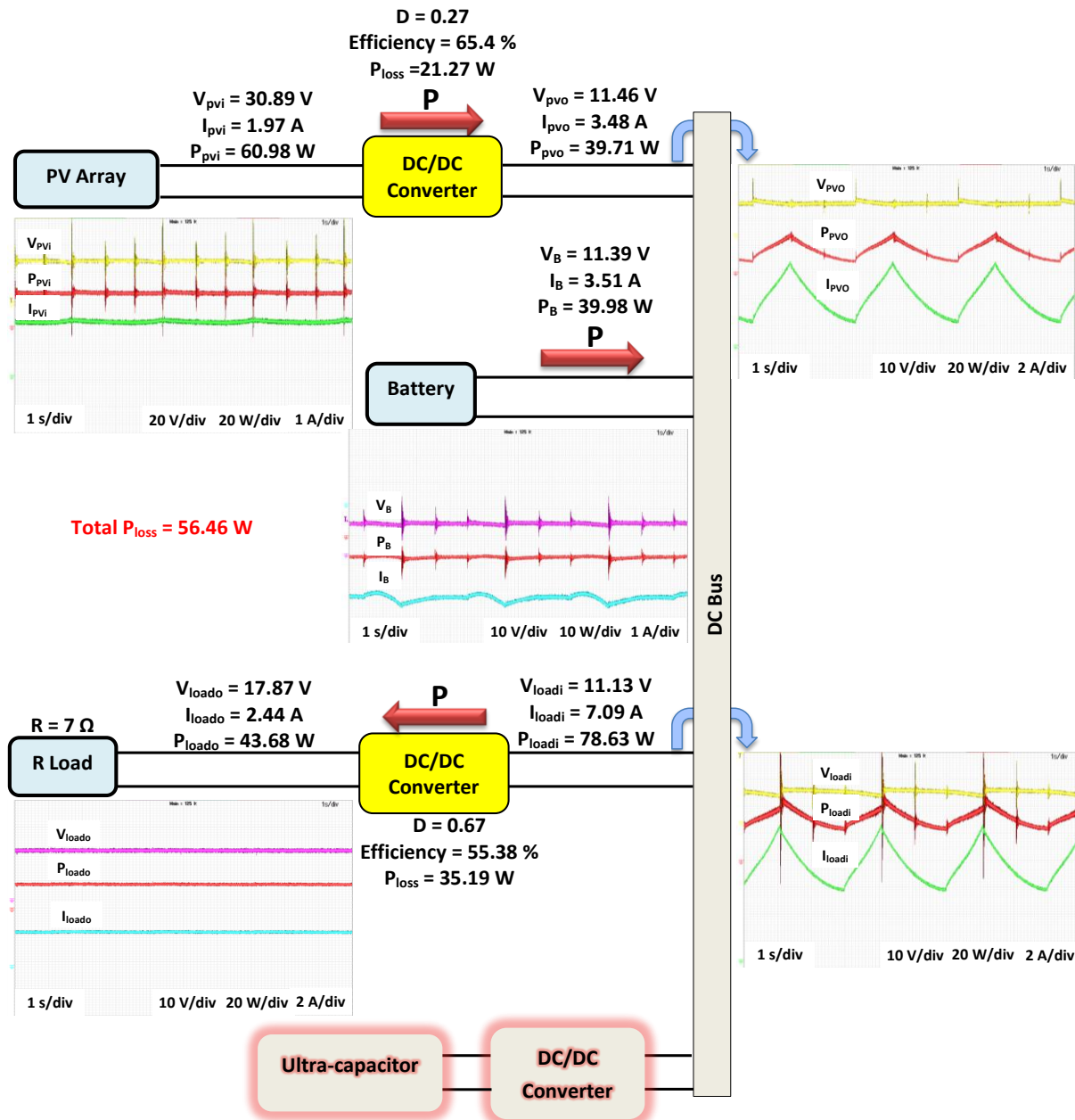


Figure 5-12 Discharging case single line diagram.

As can be seen from Figure 5-12, the output voltage of the converter connected between the battery and the resistive load is not 24 V as expected, this is due to the parasitic elements of the resistive load, coils, and capacitors that have a major effect on the system output.

C. Case 3:

The third case that is considered is shown in Figure 5-13 where the following are the operating conditions:

- 1) The PV power is equal to zero.
- 2) The battery has a state of charge which is: $SoC_L \leq SoC \leq SoC_H$ ($20\% SoC \leq SoC \leq 80\% SoC$), and the voltage of the battery is within the specified limits, where: $V_{BL} \leq V_B \leq V_{BH}$ ($10 V \leq V_B \leq 14 V$).

3) The ultra-capacitors have not connected to the system yet.

In this case the results are taken such that the PV is not operating at the MPP and the duty cycle of the converter connected between the PV panel and the battery is set to 0.23 so that the output power of the PV is zero. In other words, the PV is operating at the open circuit voltage. The Buck-Boost converter connected between the battery and the resistive load is set to a duty cycle equal to 0.67, so that the output voltage of this converter is double the input voltage. According to the operating conditions mentioned earlier, the battery is the only source that will be able to feed the load. This case is taken assuming that it is at night, where the battery will discharge to feed the load. The results are shown in the following single line diagram where the efficiency of each converter and the power losses are stated, as well as the operating voltage, current, and power for each source.

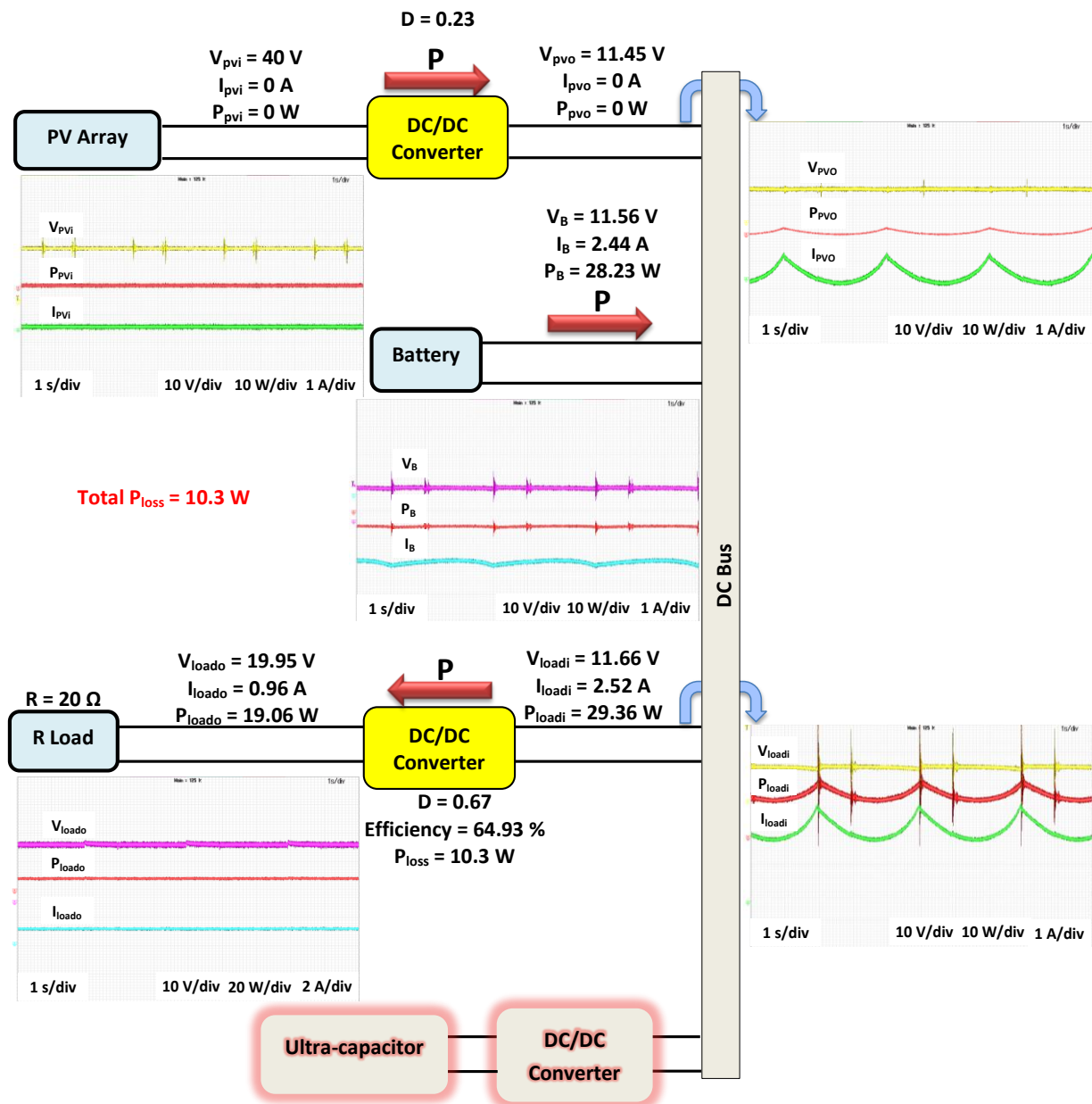


Figure 5-13 Discharging case single line diagram where the PV power is zero and the battery is discharged to feed the load.

As can be seen from Figure 5-13, the input power of the PV is zero and the battery is discharged to feed the resistive load. It is observed that the power drawn from the battery is approximately 29 W, however, the output power at the load side is 19 W, and so the power loss is 10 W.

It is clearly seen that the efficiency of the converter does not exceed 70%, and this is due to the same reasons that are mentioned in case 1, therefore, it can be said that all of the reasons that are mentioned earlier are valid for all the tested energy management cases.

It is clearly noticeable that the load output voltage is not 24 V as expected, and this is due to the effect of the parasitic elements in the designed converter that has a major effect in this voltage drop.

D. Case 4:

The fourth case that is considered is shown in Figure 5-14, where the following are the operating conditions:

- 1) The PV is not connected to the system.
- 2) The battery has a state of charge which is: $SoC_L \leq SoC \leq SoC_H$ ($20\% SoC \leq SoC \leq 80\% SoC$), and the voltage is within the specified limits, where: $V_{BL} \leq V_B \leq V_{BH}$ ($10 V \leq V_B \leq 14 V$).
- 3) The ultra-capacitors are connected to the system through a Buck-Boost converter where the current voltage of the ultra-capacitors is 15 V which is 1.2 V away from its rated voltage.

According to the constraints mentioned in section 2.5, that a dead or badly depleted battery is considered to be the extreme failure in solar car racing, thus a battery management is actually significant, since with an exhausted battery, a team has no choice other than slowing down to let the solar array recharge it. Thus, to supply sufficient energy for peak power requirements, and so do, the battery will only supply continuous power at nominal rate; it is decided to couple the ultra-capacitors with the battery to avoid deep discharge through high current for short instants, which will reduce the battery's lifetime. In addition, ultra-capacitors have high charging capabilities which make them well suited for regenerative applications. Therefore, to obtain an optimal energy management system for a solar car with high efficiency and to meet the standards mentioned in section 2.5, it is important to maintain high SoC of the battery and avoid deep discharge to reduce the damage mechanism rate of the battery pack and hence this will result in a secured and a safe system.

In this case, the PV is not connected to the system, and the ultra-capacitors replaced the load such that the battery will charge the ultra-capacitors. A series power resistor of 3 Ω is used between the output of the converter and the ultra-capacitors for protection purposes. This is due to the fact that ultra-capacitors have very high charging capabilities. The Buck-Boost converter connected between the battery and the ultra-capacitors is set to a duty cycle equals to 0.67 so that the load voltage equal to 24 V. The results are shown in the following single line diagram where the efficiency of each converter and the power losses are stated, as well as the operating voltage, current, and power for each source.

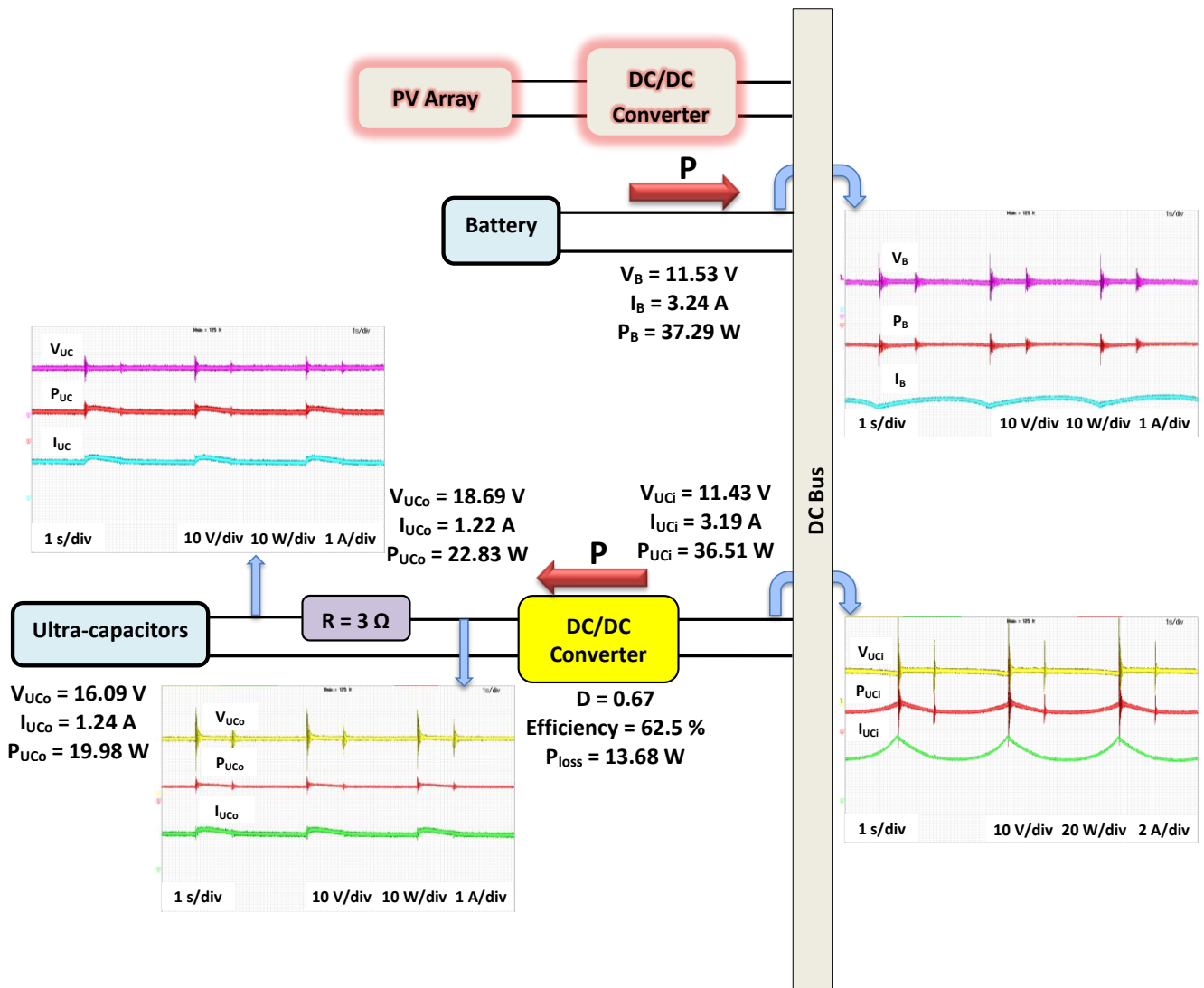


Figure 5-14 Discharging case single line diagram where the battery is charging the ultra-capacitors.



Figure 5-15 Ultra-capacitor's voltage before and after charging.

As can be seen from Figure 5-14, the battery is discharged to charge the ultra-capacitors from 15 V to 16 V through a Buck-Boost converter. It is clearly noticeable that the efficiency is low and this is due to the same reasons mentioned in the previous cases. The duty cycle is set based on the expected voltage difference between the converter and the ultra-capacitors such that the current flowing into the ultra-capacitors is no more than 3 A, however, the output voltage of the converter is dropped due to the non-idealities of the components to 18.69 V which will allow current of 1.23 A to flow into the ultra-capacitors. Figure 5-15, shows the voltage of the ultra-capacitors before and after charging.

5.6.4 Performance Assessment:

Performance assessment is done in order to observe the effect of varying the load on the voltage, current, and power at each node in the system, as well as the efficiency of each converter.

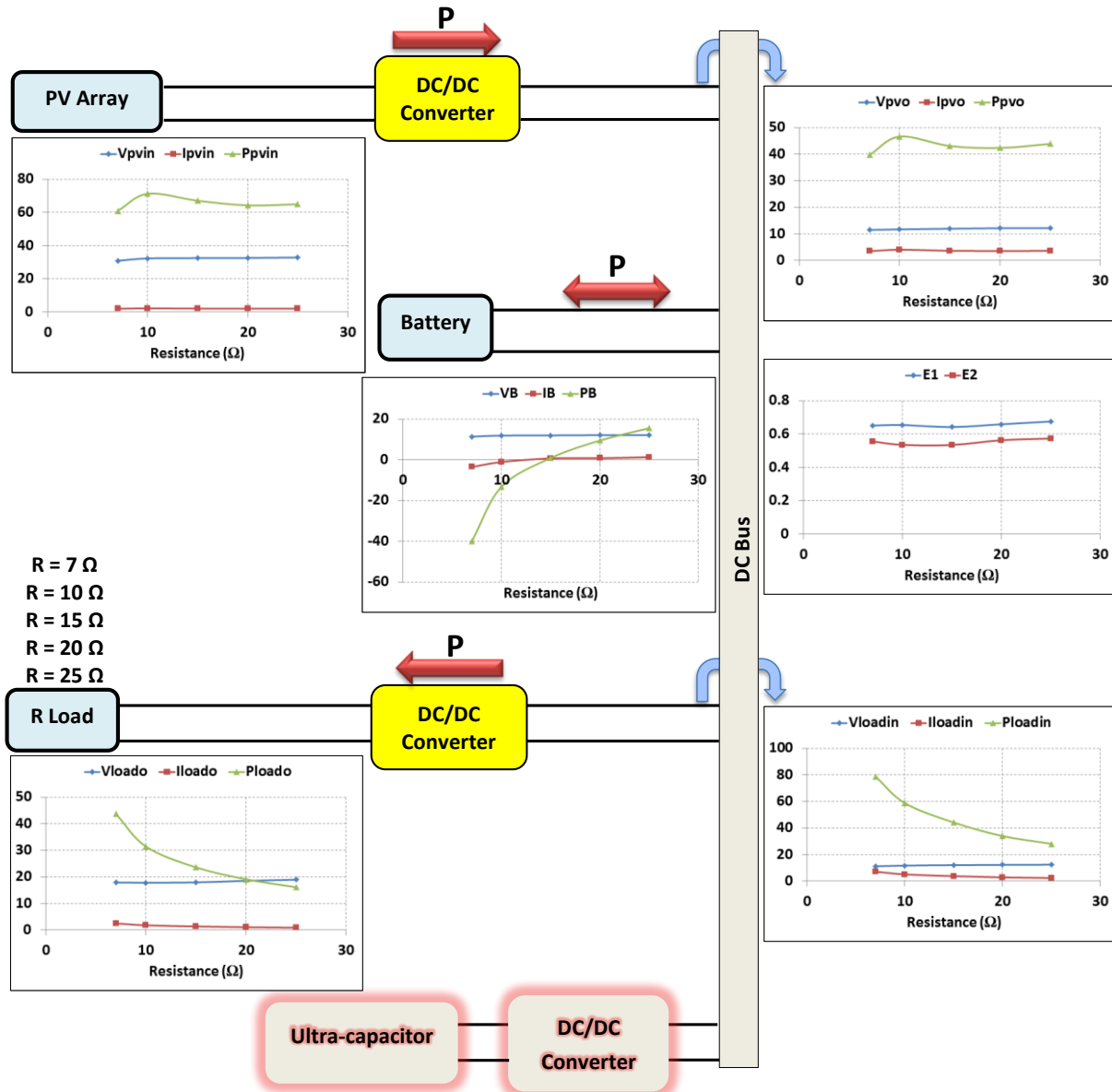


Figure 5-16 Single line diagram showing performance assessment for the energy management.

It is noticed that by increasing the value of the resistive load, the voltage, current, and power trends of the PV before and after the DC/DC converter are almost the same; the voltage is slightly increasing, and the current is almost constant. The results are taken such that the PV power does not vary. The voltage and current of the battery are increasing as the resistance increases, and so do the power, since the battery is transitioning from discharging to charging mode as the load decreases. The trend shown in Figure 5-16 for the battery as the load decreases is actually valid for all batteries regardless their type, or size; when there is current that is flowing across the cell during the charging cycle, this will lead the cell's voltage to increase, and if the current is high, the voltage will increase in a faster

manner. However, during the discharging cycle, the cell's voltage drops and this is because of the discharging current, and as the current discharging rate is higher, the voltage will decrease in a faster manner.

The voltage, current, and power trends of the load before and after the DC/DC converter behaves similarly by decreasing the load; the voltage is increasing, the current is decreasing, and therefore the power is decreasing as well.

It is clearly noticed from Figure 5-16 that the highest efficiency for the first converter, which is the one connected between the PV panel and the battery, and the second converter, which is the one connected between the battery and the resistive load are 68 % and 57.5 % respectively.

5.7 Project's Cost

The table below shows briefly the cost of this project.

Table 5-2 Project's cost.

Component	Quantity	Cost
PV Panel	1	550 \$
Battery	1	140 \$
Ultra-capacitors	1	200 \$
DSP	1	550 \$
Gate Driver Circuit	2	100 \$
IGBTs	4	20 \$
Passive elements / Heat sinks / Miscellaneous	-	100 \$
Total		1660 \$

5.8 Design Limitations

In this section, the projects' design limitations are listed showing the problems that are faced during the design process. Solutions are proposed to reduce the problems and to achieve minimal error with lower power losses and higher efficiency.

- Parasitic elements: parasitic elements in the coils, resistors, inductors, and capacitors have major effects on the output of the system.
- Low efficiency: using IGBTs at high switching frequency equal to 50 kHz results in low efficiency. Thus, it is suggested to use MOSFETs instead of the IGBTs since they have higher switching capabilities, or to work at a lower switching frequency.
- Silicon devices instead of Silicon Carbide devices: System efficiency is considered to be an important criterion in evaluating the system performance. To maximize the power capability, minimize the losses, and achieve higher switching frequency; devices based on wide band gap material such as Gallium Nitride (GaN) and Silicon Carbide (SiC) are considered to be the solution to avoid Silicon (Si) limitations. The employment of SiC devices in power converters introduces higher power density, lower losses, and higher operating temperature when compared to Si devices.

- Ripples and oscillations: It is clearly noticeable that all the obtained results have ripples and underdamped oscillations. This is due to the improper wiring that results in stray inductance which is actually an unwanted inductance. To avoid this effect, it is preferable to use short stranded wires to avoid any noise. In addition, the use of capacitors at each power entry will filter out the noise. Moreover, the usage of coaxial cables and bus bars will minimize the ripples.
- Ultra-capacitors closed loop operation: ultra-capacitors charge and discharge in a very fast way, hence complying with the standards mentioned in section 2.5 which state that monitoring system should be carefully designed for all storage devices to ensure safety and so do a current controlled loop should be designed to control the inflow and the outflow between the ultra-capacitors and the DC bus.
- Low DC voltage bus: the system is designed such that the DC bus voltage is 48 V, however, practically the DC bus is 12 V. Accordingly, at high power operating conditions, high current is drawn from the storage devices. Thus, it is suggested to work at high voltage DC bus to avoid high current.

Chapter 6 : CONCLUSION AND FUTURE WORK

Solar car racing has raised the interest of energy issues and research topics in the public domain. In addition, it has great consequences on the electric vehicles' development. To achieve the best system optimization, it is highly required to understand the system vehicle electrical system. In this project, three different sources are used to transfer power according to the motor requirements which are PV modules, Li-ion battery, and ultra-capacitors.

Photovoltaic technology is expanded widely in many power applications. In solar races, it is very important to select PV modules with high efficiency; however, there is a trade-off between efficiency and cost, but since the aim is to compete in the upcoming world solar challenge events; the cost factor comes as a second priority as PV modules with high efficiency provide higher output power.

Weight and capacity are the most important criteria for solar car battery selection, since more weight increases the rolling resistance, hence more power will be needed to drive the car. In addition, managing the content of the battery is an important factor affecting the energy management of the solar car, since temperature and the level of discharge affect the actual capacity of a lithium ion battery and its lifetime.

The performance of a solar powered vehicle is improved by using ultra-capacitors as a second energy storage device with the other two power sources (PV + Battery), since ultra-capacitors are characterized by their high power, low internal resistance, capability of quick charge with high current and deep discharge, and their performance under a wide temperature range. Nevertheless, ultra-capacitors have low energy density unlike batteries. Thus, a more practical way is using a battery with ultra-capacitors, where each energy storage device will perform its own duty based on its characteristics and the current circumstances.

The aim of this project is to develop the energy management system of a solar powered car that includes three power sources. The solar panels convert the absorbed solar energy into electrical energy under maximum power point strategy during the day to transfer power to the load and the battery. The battery feeds the power demand by the brushless DC motor, and the ultra-capacitors are used during frequent starts and stops.

To design a lightweight, and a highly efficient solar powered car, monocrystalline PV modules, lithium ion battery, and in-wheel axial flux permanent magnet brushless DC motor are selected. Monocrystalline PV modules are selected due to their high efficiency. In addition, lithium ion battery is chosen because of its high energy density, size and weight advantages, and long life cycle. Moreover, brushless DC motor is selected since they have high power to weight ratio.

From the practical implementation point of view, the energy management is accomplished with an open loop control scheme. The MPPT is implemented and tested using P&O algorithm at different perturbation sizes. In addition, different energy management cases are considered and tested under different conditions, where a battery of 12 V is directly connected to the DC bus. Moreover, performance assessment is done to observe the effect of varying the resistive load on the voltage, current, and power of each source as well as the efficiency of the two converters. It is concluded that the resulted low efficiency is due to the fact that the converters are designed for high power ratings, in addition to the losses incurred by the IGBTs and all the parasitic elements in general. Moreover, the designed DC bus is 48 V, however, practically a DC bus of 12 V is used which causes higher current to be drawn out of the battery and hence higher losses.

Future work:

- 1) As can be noticed in section 4.5.1, the implemented topology is the one where the battery is directly connected to the DC bus, such that it takes care of the steady state load as well as load's transient situations since the battery's charging and discharging rates take place in an uncontrolled fashion. To avoid the battery's voltage fluctuation, the battery charging and discharging rates can be fully controlled to ensure extended lifetime and battery health status using a controller that measures both the voltage of the battery and the SoC. Connecting the battery to the DC bus through a converter will compensate for the DC bus voltage deviation during severe disturbance conditions so that the energy is stored and managed in an efficient and optimal way. Two control methods could be considered which are the voltage mode control and the current mode control which are normally performed by proportional integral (PI) controller.
- 2) To avoid the ultra-capacitors' overcharge and discharge situations, it is preferable to add a current controlled loop.
- 3) To have a more reliable and more efficient system in the future, the concept of Multiport Power Electronic Interface MPEI can be used which is capable of interfacing and managing various sources, storage devices, and loads. To further illustrate, MPEI shown in Figure 6-1 is a multiple input power electronic converter that is capable of interfacing with different sources, storages, and loads. The concepts, analysis, and design of MPEI allow designing intelligent power electronic setup for future sustainable energy systems. A multiple-input converter can harvest and process the power from the PV panel, battery, and the ultra-capacitors as a lumped unit. MPEI enables optimal energy management. In addition, MPEI has the advantages of low cost and high power density.

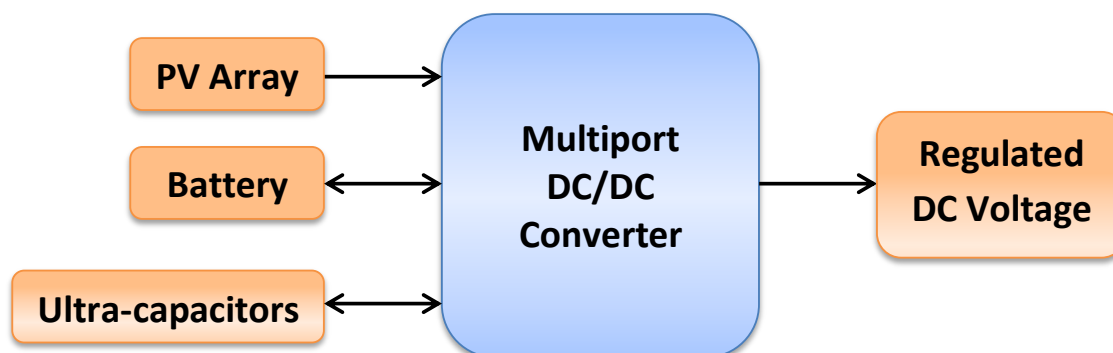


Figure 6-1 Multiport system structure.

REFERENCES

- [1] T. Altenburg, "From Combustion Engines to Electric Vehicles," 29 October 2014. [Online]. [Accessed 30 November 2015].
- [2] Y. S. Wamborikar and A. Sinha, "Solar Powered Vehicle," *Proceedings of the World Congress on Engineering and Computer Science 2010 Vol II*, 20 - 22 October 2010.
- [3] D. T. Wisniewski, "Solar flair: An open-road challenge," pp. 6 - 9, January - February 2010.
- [4] Z. Taha, R. Passarella and J. M. Sah, "A Review on Energy Management system of Solar Car," in *Proceedings of the 9th Asia Pasific Industrial Engineering & Management Systems Conference*, Malaysia, 2008.
- [5] "The history reminder - The First Solar Car," 20 September 2012. [Online]. Available: <http://www.energy-today.biz/en/history-reminder-first-solar-car/>. [Accessed 10 October 2015].
- [6] "History," 1 October 2013. [Online]. Available: http://www.worldsolarchallenge.org/about_wsc_2015/history. [Accessed 1 October 2015].
- [7] R. Mangu, K. Prayaga, B. Nadimpally and S. Nicaise, "Design, Development and Optimization of Highly Efficient Solar Cars: Gato del Sol I-IV," *Green Technologies Conference, 2010 IEEE*, pp. 1-6, 15-16 April 2010.
- [8] L. Marks, "The History of Solar Car Racing," 2015. [Online]. Available: <http://www.solarcarchallenge.org/challenge/history.shtml>. [Accessed 11 October 2015].
- [9] "1987 GM Sunraycer Solar car," 10 November 2011. [Online]. Available: <http://ecomodder.com/forum/member-sven7-albums-aero+vehicles-picture3226-1987-gm-sunraycer-solar-car.html>. [Accessed 10 October 2015].
- [10] "Overview," 5 June 2014. [Online]. Available: http://www.worldsolarchallenge.org/page/view_by_id/76. [Accessed 10 October 2015].
- [11] "2015 Classes," 19 October 2015. [Online]. Available: http://www.worldsolarchallenge.org/team_info/2015_classes. [Accessed 10 October 2015].
- [12] "Honour Roll," 4 June 2014. [Online]. Available: http://www.worldsolarchallenge.org/about_wsc_2015/history/honour_roll. [Accessed 10 October 2015].
- [13] A. Mills and E. Stumpges, "The American Solar Challenge 2012," *IEEE POTENTIALS*, pp. 10 - 16, 26 March 2013.

- [14] S. Said, A. Massoud, M. Benammar and S. Ahmed, "A Matlab/Simulink-Based Photovoltaic Array Model Employing SimPowerSystems Toolbox," *Journal of Energy and Power Engineering*, vol. 6, pp. 1 - 11, 31 December 2012.
- [15] M. A. Maehlum, "Solar Cell Comparison Chart – Mono-, Polycrystalline and Thin Film," Energy Informative, 27 September 2013. [Online]. Available: <http://energyinformative.org/solar-cell-comparison-chart-mono-polycrystalline-thin-film/>. [Accessed 15 October 2015].
- [16] "Battery Types," Canadian Automobile Association, 2015. [Online]. Available: <http://electricvehicles.caa.ca/types-of-electric-vehicles/battery-types/>. [Accessed 6 October 2015].
- [17] N. Alnunu, S. Said, . S. Al-Sharman, A. Al-Ibrahimi , . A. AbdulAzi, M. Al Hellabi , F. Touati, . S. Ghani, E.-S. Mahdi and . M. Benammar, "Design of Qatar University's First Solar Car for Shell Eco-Marathon Competition," *Renewable Energies and Vehicular Technology (REVET), 2012 First International Conference* , pp. 49 - 54, 26 - 28 March 2012.
- [18] A. Spohn, "Lead-acid battery safety," University of, 2015. [Online]. Available: <https://www.wisconsin.edu/ehs/osh/battery-safety/>. [Accessed 6 October 2015].
- [19] Y. Xing, E. Ma, K. Tsui and M. Pecht, "Battery Management Systems in Electric and Hybrid Vehicles," *Energies 2011*, vol. 4, pp. 1 - 18, 21 October 2011.
- [20] B. Wu, F. Zhuo, . F. Long, W. Gu and Y. Q, "A management strategy for solar panel –battery–super capacitor hybrid energy system in solar car," *8th International Conference on Power Electronics - ECCE Asia*, pp. 1682 - 1687, 30 - 3 May - June 2011.
- [21] G. Zorpette, "Sun Kings cross the outback [solar powered vehicles marathon]," *Spectrum, IEEE*, vol. 39, no. 2, pp. 40-46, February 2002.
- [22] "2015 Regulations," 2015 April 2015. [Online]. Available: http://www.worldsolarchallenge.org/team_info/2015_regulations. [Accessed 1 October 2015].
- [23] F. A. O. Aashoor and F. V. P. Robinson, "A Variable Step Size Perturb and Observe Algorithm for Photovoltaic Maximum Power Point Tracking," *Universities Power Engineering Conference (UPEC), 2012 47th International* , pp. 1 - 6, 4 - 7 September 2012.
- [24] A. K. Abdelsalam, . A. M. Massoud, S. Ahmed and P. N. Enjeti, "High-Performance Adaptive Perturb and Observe MPPT Technique for Photovoltaic-Based Microgrids," *Power Electronics, IEEE Transactions*, vol. 26, no. 4, pp. 1010 - 1021, April 2011.
- [25] L. Piegari and R. Rizzo, "Adaptive perturb and observe algorithm for photovoltaic maximum power point tracking," *Renewable Power Generation, IET*, vol. 4, no. 4, pp. 317 - 328, July 2010.
- [26] N. Femia, G. Petrone, G. Spagnuolo and M. Vite, "Optimization of perturb and observe maximum

- power point tracking method," *Power Electronics, IEEE Transactions*, vol. 20, no. 4, pp. 963 - 973, July 2005.
- [27] A. M. Atallah, A. Y. Abdelaziz and R. S. Jumaah, "IMPLEMENTATION OF PERTURB AND OBSERVE MPPT OF PV SYSTEM WITH DIRECT CONTROL METHOD USING BUCK AND BUCK-BOOST CONVERTERS," *Emerging Trends in Electrical, Electronics & Instrumentation Engineering: An international Journal*, vol. 1, no. 1, pp. 31 - 44, February 2014.
- [28] M. A. Maehlum, "Which Solar Panel Type is Best? Mono- vs. Polycrystalline vs. Thin Film," *Energy Informative*, 18 May 2015. [Online]. Available: <http://energyinformative.org/best-solar-panel-monocrystalline-polycrystalline-thin-film/>. [Accessed 15 October 2015].
- [29] D. Sulaiman, H. Ameen and I. Said, "Design of High Efficiency DC-DC Converter for Photovoltaic Solar Home Applications," *Journal of Energy and Power Engineering*, vol. 4, no. 11, pp. 43 - 51, 30 November 2010.
- [30] M. . H. TUSHAR, "COMPARATIVE STUDY ON DC-DC CONVERTERS," [Online]. Available: <http://dSPACE.bracu.ac.bd/bitstream/handle/10361/1746/Mehedi%20Hasan%20Tusher.pdf?sequence=1>. [Accessed 20 November 2015].
- [31] "Switched Mode Power Supplies," [Online]. Available: <http://www.learnabout-electronics.org/Downloads/Power%20Supplies%20Module%2003.pdf>. [Accessed 20 November 2015].
- [32] J. Zhang, "Bidirectional DC-DC Power Converter Design Optimization, Modeling and Control," 30 January 2008. [Online]. Available: http://scholar.lib.vt.edu/theses/available/etd-02052008-122048/unrestricted/Dissertation_jhz.pdf. [Accessed 20 December 2015].
- [33] "Lithium-ion Battery and Energy," BYD Company Limited. [Online]. [Accessed 12 December 2015].
- [34] D. Menasce, M. Grobler and P. . J. v. Rensburg, "High Power Electrical Systems Design for a Solar Car Designing and building the solar car llangal.I," *AFRICON, 2013*, pp. 1 - 5, 9 - 12 September 2013.
- [35] R. Al Zaher, S. de Groot, H. Polinder and P. Wieringa, "Comparison of an axial flux and a radial flux permanent magnet motor for solar race cars," *Electrical Machines (ICEM), 2010 XIX International Conference*, pp. 1 - 6, 6 - 8 September 2010.
- [36] R. Qu, M. Aydin and T. A. Lipo, "Performance Comparison of Dual-Rotor Radial-Flux and Axial-Flux Permanent-Magnet BLDC Machines," pp. 1 - 8.
- [37] Y. ITOH, K. SAKAI and Y. MAKINO, "In-Wheel Motor System," 2011. [Online].
- [38] "In-wheel motor," NISAN MOTOR CORPORATION, [Online]. Available: <http://www.nissan->

global.com/EN/TECHNOLOGY/OVERVIEW/in_wheel_motor.html. [Accessed 2 November 2015].

- [39] A. Scheidegger, "Energy Management Optimization for a Solar Vehicle," 26 February 2006. [Online]. Available: <http://transp-or.epfl.ch/documents/masterTheses/SCHEIDEGGER06.pdf>. [Accessed 25 December 2015].
- [40] A. Tani, M. B. Camara and B. Dakyo, "Energy Management Based on Frequency Approach for Hybrid Electric Vehicle Applications: Fuel-Cell/Lithium-Battery and Ultracapacitors," *IEEE TRANSACTIONS ON VEHICULAR TECHNOLOGY*, vol. 61, no. 8, pp. 3375 - 3386, October 2012.
- [41] "SPECTRUM DIGITAL EZDSP F28335 Development Kit, TMS320F28335, With CC Studio, 16bit Colour Display, Onboard J-TAG Emulator," Premier Farnell , 2016. [Online]. Available: <http://canada.newark.com/spectrum-digital/ezdsp-f28335/tms320f28335-rs232-can-w-cc-studio/dp/78R2979>. [Accessed 5 March 2016].

Appendix A TABLES

Table A-1 Third design of the Buck-Boost converter for PV.

Case 3			
Given		Required	
V_{in} (V)	57.6	D	0.455
P_{in} (kW)	1.035	R (Ω)	2.226
I_{in} (A)	17.969	I_L (A)	39.531
V_o (V)	48	L_{design} (μ H)	165.5
P_o (kW)	1.035	v_L (V)	57.6
I_o (A)	21.563	$\Delta i_{L,new}$ (A)	3.1625
Assumed		$I_{L,rms}$ (A)	39.626
f_s (kHz)	50	C_{design} (μ F)	408.381
T_s (μ s)	20	$V_r/V_{o_{new}}$ (%)	1
Δi_L (A)	3.953	V_C (V)	48
V_r/V_o (%)	2	V_d (V)	105.6
		V_s (V)	105.6

Table A-2 Prototype design of the Buck-Boost converter for PV.

Prototype Design			
Given		Required	
V_{in} (V)	30	D	0.615
P_{in} (W)	200	R (Ω)	11.520
I_{in} (A)	6.667	I_L (A)	10.833
V_o (V)	48	L_{design} (μ H)	142.012
P_o (W)	200	v_L (V)	48
I_o (A)	4.167	$\Delta i_{L,new}$ (A)	2.6
Assumed		$I_{L,rms}$ (A)	11.065
f_s (kHz)	50	C_{design} (μ F)	213.675
T_s (μ s)	20	$V_r/V_{o_{new}}$ (%)	0.5
Δi_L (A)	3.250	V_C (V)	48
V_r/V_o (%)	1	V_d (V)	78
		V_s (V)	78

Appendix B FIGURES

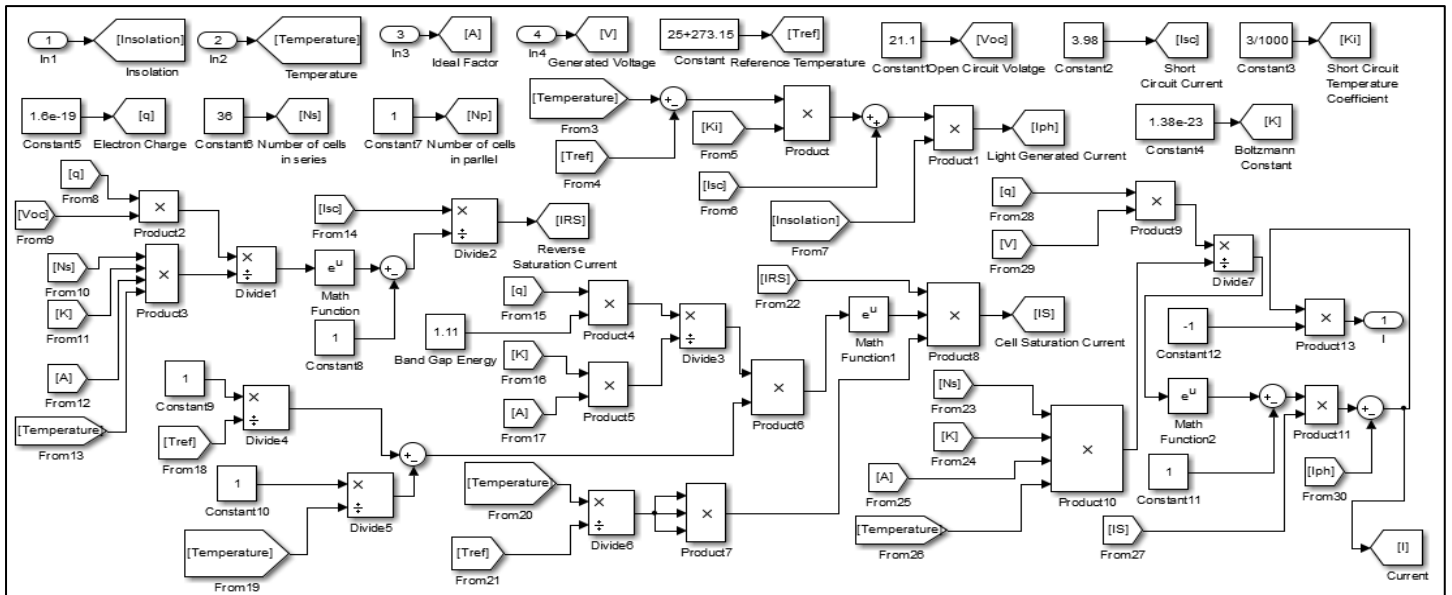


Figure B-1 Simulink mathematical modeling of the simplified PV module.

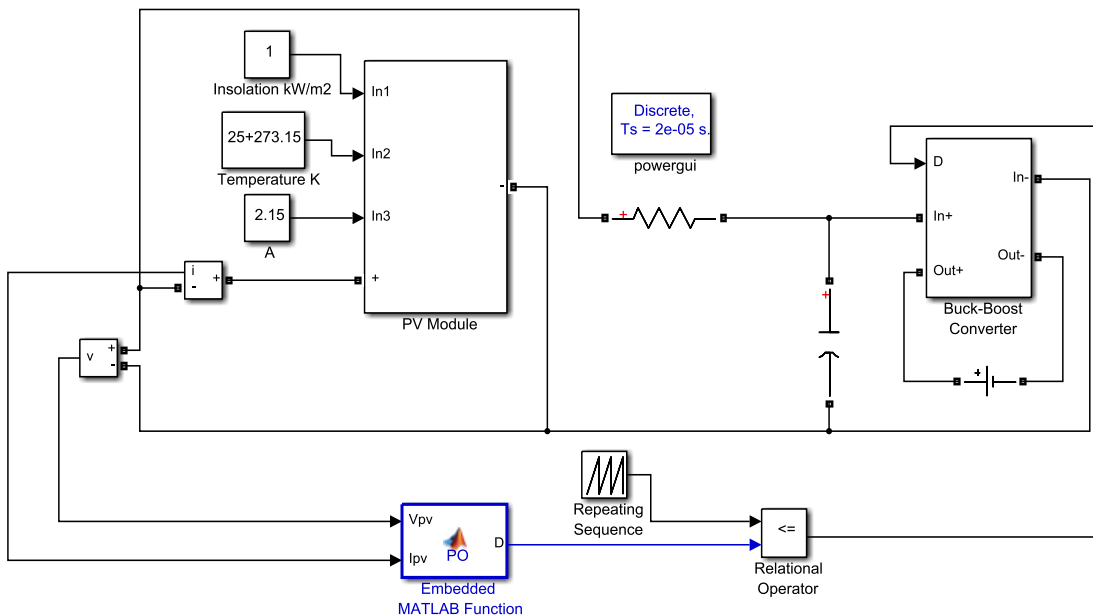


Figure B-2 PV model with the MPPT using P&O method.

```

function D = PO(Vpv, Ipv)

persistent D_old V_old P_old

if isempty(D_old)
    D_old = 0.3;
    V_old = 0;
    P_old = 0;
end

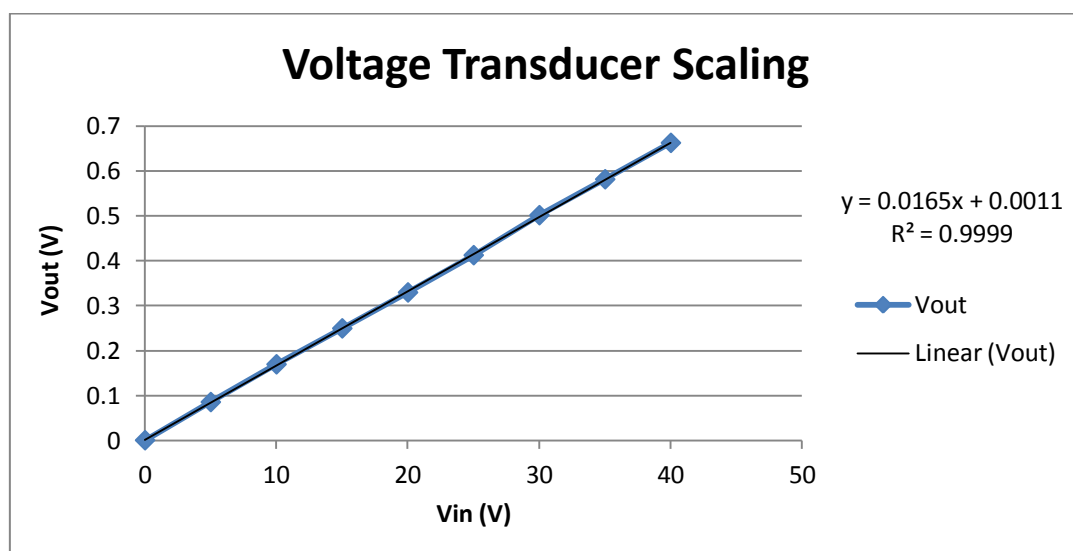
delD = 0.01;
Ppv = Vpv * Ipv;

if (Ppv - P_old) > 0
    if (Vpv - V_old) > 0
        D = D_old - delD;
    else
        D = D_old + delD;
    end
else
    if (Vpv - V_old) > 0
        D = D_old + delD;
    else
        D = D_old - delD;
    end
end

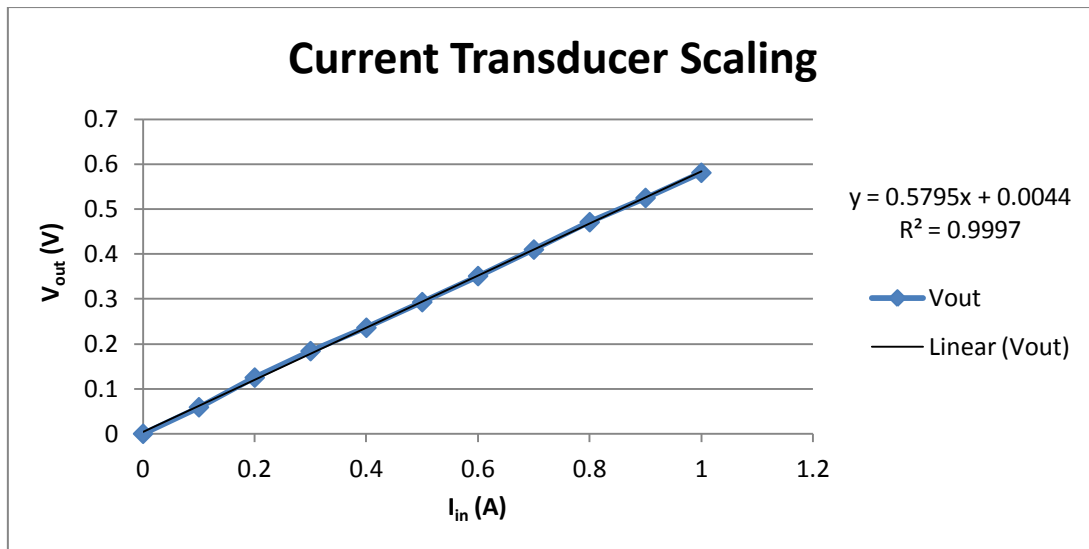
D = D_old ;
Vpv = V_old;
Ppv = P_old ;

```

Figure B-3 MPPT Matlab code using P&O algorithm.



(a)



(b)

Figure B-4 Transducer's calibration process: (a) Voltage transducer scaling; (b) Current transducer scaling.